Journal of the Meteorological Society of Japan, Vol. 75, No. 4, pp. 775–797, 1997

United Mechanisms for the Generation of Low- and High-Frequency Tropical Waves. Part II: Theoretical Interpretations

By Y. Hayashi and D.G. Golder

Geophysical Fluid Dynamics Laboratory/NOAA Princeton University, P.O. Box 308, Princeton, New Jersey 08542, USA

(Manuscript received 4 September 1996, in revised form 11 April 1997)

Abstract

It is assumed that low- and high-frequency tropical waves are generated by the united mechanisms consisting of the evaporation-wind feedback (EWF), saturation-triggering (ST), and lateral-triggering mechanisms. Through the EWF mechanism, some waves become unstable owing to evaporation-wind feedback. Through the ST mechanism, other waves are triggered by the intermittent onset of moist convection, upon saturation, to neutralize any pre-existing conditionally unstable stratification. These mechanisms are theoretically interpreted by partitioning moist convective adjustment into two consecutive processes of *diagnostic* and *prognostic* adjustments. The two processes respectively restore and maintain convective equilibrium, and are crucial to the ST and EWF mechanisms.

As a step to toward a unified theory, EWF instability is examined by the use of a theoretical Kelvin-wave model, which incorporates only the prognostic-adjustment process in the linearized perturbation equations, thereby excluding the ST mechanism. The solutions indicate that wave instability results from the EWF mechanism and not from the wave-CISK mechanism. For a plausible choice of adjustable parameters, one strongly unstable mode corresponds to the observed 40–50-day oscillation, while two weakly unstable modes correspond to the observed 25–30- day and 10–20-day oscillations.

These results are compared with those from the numerical experiments conducted in Part I, using a nonlinear model incorporating the original moist convective adjustment scheme. It is then speculated that the 40–50- and 25–30-day modes can strongly grow through the linear and nonlinear EWF mechanisms respectively, while the 10-20-day mode can strongly amplify through the ST mechanism.

1. Introduction

In order to explain the generation of both low- and high-frequency tropical waves, Hayashi and Golder (1994) proposed the "united mechanisms" which consist of the evaporation-wind feedback (EWF) mechanism, "saturation-triggering (ST) mechanism", and the lateral-forcing mechanism. Through the EWF mechanism (Neelin *et al.*, 1987; Emanuel, 1987), tropical intraseasonal oscillations coupled with moist convection become unstable owing to evaporation-wind feedback. Through the ST mechanism (Hayashi and Golder, 1994), other transient waves are triggered by the intermittent onset of moist convection, upon saturation, to neutralize any pre-existing unstable stratification that has developed during periods of nonsaturation.

To examine the united mechanisms, numerical experiments were conducted in Part I (Hayashi and Golder, 1997), using an idealized 9-level R21-spectral model with the original scheme of moist convective adjustment (MCA). This model produced tropical intraseasonal oscillations (TIOs), Kelvin and mixed Rossby-gravity (MRG) waves, and superclusters. The results from the numerical experiments were consistent with the united mechanisms. For example, TIOs were maintained primarily through the EWF feedback mechanism. Other waves were maintained primarily through the ST mechanism and/or the lateral-triggering mechanism. In particular, when both the EWF and ST mechanisms were removed, all tropical transient waves disappeared, in spite of the presence of the moisture-convergence feedback process. This result is contrary to the wave-CISK mechanism (Hayashi, 1970), through which tropical transient waves coupled with moist convection become unstable, even in the absence of evaporation-wind feedback. It is, however, consistent with convective cancellation (Emanuel, 1987) based on the convective-neutrality hypothesis and EWF instability theory (Neelin and

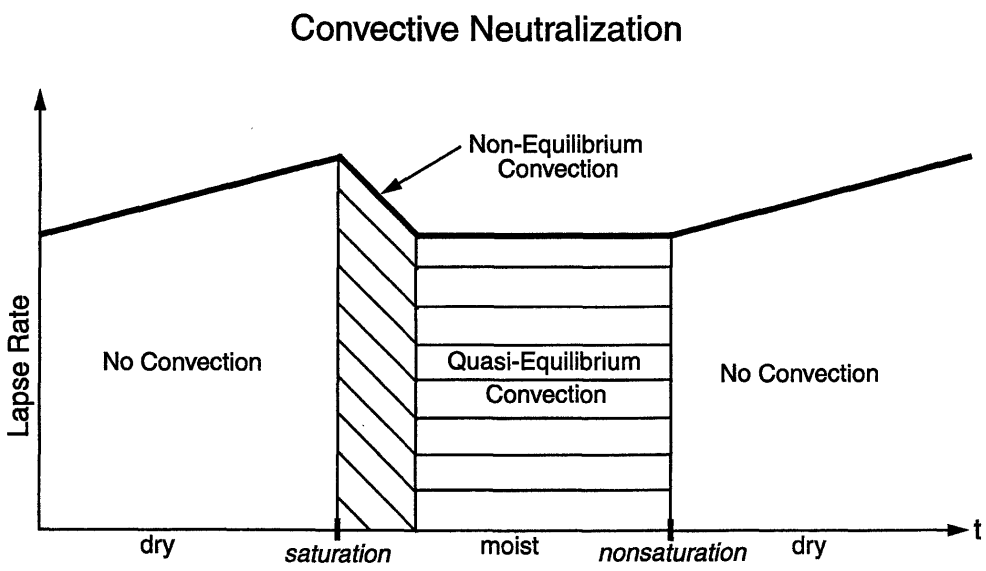

Fig. 1. Schematic of the effect of moist convection on the neutralization of static stability as a function of time.

Yu, 1994; Yu and Neelin, 1994) based on the Betts-Miller parameterization (Betts and Miller, 1986).

As schematically illustrated in Fig. 1, the MCA process can be conceptually interpreted as follows. It is hypothesized that moist convection is initiated upon saturation and rapidly grows in the presence of pre-existing unstable stratification. The growing "non-equilibrium" convection quickly becomes "quasi-equilibrium" convection and is maintained during periods of saturation until it is dissipated upon nonsaturation. The MCA hypothesis crucially differs from the quasi-equilibrium hypothesis (Arakawa and Schubert, 1974) and the convective-neutrality hypothesis (Emanuel, 1987) in that the MCA scheme turns off moist convection during periods of nonsaturation, allowing conditionally unstable stratification to develop during these periods.

The MCA process can be conceptually partitioned into two consecutive processes of "diagnostic" and "prognostic" adjustments that represent the effects of convection in the growing and mature stages, respectively. Diagnostic adjustment intermittently neutralizes, upon saturation, any pre-existing unstable stratification, thereby restoring convective equilibrium. Prognostic adjustment continually neutralizes, during saturation, any predicted unstable stratification, thereby maintaining the restored convective equilibrium. As demonstrated by numerical experiments in Part I, diagnostic adjustment is crucial to the ST mechanism, while prognostic adjustment is crucial to the EWF mechanism. In the present paper, these mechanisms are theoretically interpreted in terms of these adjustment processes.

In Section 2, the MCA scheme is mathematically partitioned into diagnostic- and prognostic-adjustment schemes. Section 3 examines evaporation-wind feedback instability by use of a theoretical Kelvin-wave model that incorporates only the prognostic adjustment scheme, thereby eliminating the ST mechanism. Section 4 interprets the theoretical results, while Section 5 dynamically interprets the ST mechanism. Section 6 is devoted to conclusions and remarks.

2. The partitioned scheme of moist convective adjustment

The original scheme of moist convective adjustment (Manabe *et al.*, 1965) assumes that the conditionally (*i.e.*, moist-adiabatically) unstable stratification and super-saturated humidity, which are predicted prior to MCA for a small time-increment, are instantaneously adjusted to the conditionally neutral and saturated values. This occurs in such a way that the sum of latent and sensible heating due to MCA is zero upon vertical integration. It is also assumed that the kinetic energy of convection is instantaneously dissipated, while all the condensed water is instantaneously precipitated.

The instantaneous adjustment scheme of MCA was modified by Betts (1986) and Betts and Miller (1986) so that temperature and humidity are gradually restored through a relaxation process, to either the moist adiabatic and saturation values or to observed vertical distributions. Reviews of convective parameterization schemes can be found in Arakawa and Chen (1987), Arakawa (1993), Emanuel and Raymond (1993), Emanuel (1994), and Emanuel *et al.* (1994).

In this section, the original scheme of MCA is rederived and then partitioned into "diagnostic" and

"prognostic" adjustment processes. The continuous scheme for MCA is obtained as the limit for an infinitesimal time increment. The heating and moistening due to the two processes are explicitly determined in terms of large-scale variables.

In the following, the log-pressure coordinate system is used in the governing equations. Most of the symbols used are listed in Appendix A. The explicit expressions for the partitioned scheme are derived in Appendix B.

2.1 The discrete scheme of MCA

The temperature and moisture balance equations can be written in vector form as

$$\frac{\partial \boldsymbol{H}}{\partial t} = \boldsymbol{F} + \boldsymbol{Q}_a. \tag{2.1}$$

Here, the vectors consist of the temperature and moisture components as

$$\boldsymbol{H} = (C_pT, Lq), \tag{2.2a}$$
$$\boldsymbol{F} = (F_T, F_q), \tag{2.2b}$$

and

$$\boldsymbol{Q}_a = (Q_T, Q_q), \tag{2.2c}$$

where T and q are the temperature and moisture, respectively. F_T and F_q are the respective heating and moistening rates which are not due to MCA, while Q_T and Q_q are the respective heating and moistening rates resulting from MCA.

Integration of (2.1) over a time increment Δt yields

$$\boldsymbol{H}(t+\Delta t) = \boldsymbol{H}(t) + (\tilde{\boldsymbol{F}} + \tilde{\boldsymbol{Q}}_a)\Delta t, \tag{2.3}$$

where the tilde ($\tilde{}$) denotes the time average between t and $t+\Delta t$.

Setting $\tilde{\boldsymbol{Q}}_a = 0$ in (2.3) results in $\hat{\boldsymbol{H}}$, which is the value of $\boldsymbol{H}$ temporarily predicted at $t+\Delta t$ without MCA as

$$\hat{\boldsymbol{H}}(t+\Delta t) = \boldsymbol{H}(t) + \tilde{\boldsymbol{F}}\Delta t. \tag{2.4}$$

i) The conditions for the occurrence of MCA are that prior to MCA, the hypothetically predicted atmosphere becomes both super-moist-adiabatic and super-saturated at $t+\Delta t$ as

$$\frac{\partial \hat{h}^*}{\partial z} < 0, \tag{2.5}$$

and

$$\hat{q} > q^*(\hat{T}, p). \tag{2.6}$$

Here, q^* is the saturated specific humidity, which is a function of temperature and pressure. The hypothetically saturated moist static energy h^* is defined in log-pressure coordinates as

$$h^* = C_pT + Lq^* + \phi, \tag{2.7}$$

where ϕ is the geopotential.

The value of $\boldsymbol{H}$ actually predicted with MCA in (2.3) is explicitly given by MCA closure as

$$\boldsymbol{H}(t+\Delta t) = \boldsymbol{H}_a(t+\Delta t), \tag{2.8}$$

where $\boldsymbol{H}_a(t+\Delta t)$ is the convectively adjusted value of $\hat{\boldsymbol{H}}(t+\Delta t)$ determined by the following set of equations:

$$\boldsymbol{H}_a(t+\Delta t) = \hat{\boldsymbol{H}}(t+\Delta t) + \tilde{\boldsymbol{Q}}_a\Delta t, \tag{2.9a}$$
$$\frac{\partial h_a(t+\Delta t)}{\partial z} = 0, \tag{2.9b}$$
$$q_a(t+\Delta t) = q^*(T_a(t+\Delta t), p), \tag{2.9c}$$

and

$$\langle \tilde{Q}_T + \tilde{Q}_q \rangle = 0. \tag{2.9d}$$

Here, the angle bracket $\langle\ \rangle$ denotes the vertical mass average over the convective layer.

ii) The conditions for the occurrence of large-scale condensation are that the atmosphere becomes supersaturated, but not super-moist-adiabatic. In this case, $\boldsymbol{H}_a$ is determined by omitting (2.9b) and replacing (2.9d) with

$$\tilde{Q}_T + \tilde{Q}_q = 0, \tag{2.9e}$$

which does not involve a vertical mass average.

iii) The condition for the occurrence of dry convective adjustment is that the atmosphere becomes dry-adiabatically unstable but not supersaturated. In this case, $\boldsymbol{H}_a$ is determined by omitting the moisture and moistening rates in the above equations.

2.2 The partitioning of MCA

It is assumed that any dry-adiabatically unstable stratification has already been neutralized by dry convective adjustment.

Equation (2.9a) yields

$$\tilde{Q}_a\Delta t = \boldsymbol{H}_a(t+\Delta t) - [\boldsymbol{H}(t) + \tilde{\boldsymbol{F}}\Delta t]. \tag{2.10}$$

The right-hand side terms can be partitioned into two consecutive processes of diagnostic ($\tilde{\boldsymbol{D}}_a$) - and prognostic ($\tilde{\boldsymbol{P}}_a$) - adjustment terms as

$$\tilde{\boldsymbol{Q}}_a = \tilde{\boldsymbol{D}}_a + \tilde{\boldsymbol{P}}_a, \tag{2.11}$$

Here, the diagnostic adjustment is defined by

$$\tilde{\boldsymbol{D}}_a\Delta_t = \boldsymbol{H}_a(t) - \boldsymbol{H}(t) \text{ for } t = t_0, \tag{2.12a}$$
$$= 0 \text{ for } t \neq t_0, \tag{2.12b}$$

where supersaturation is assumed to occur immediately after t_0.

On the other hand, the prognostic adjustment is defined by

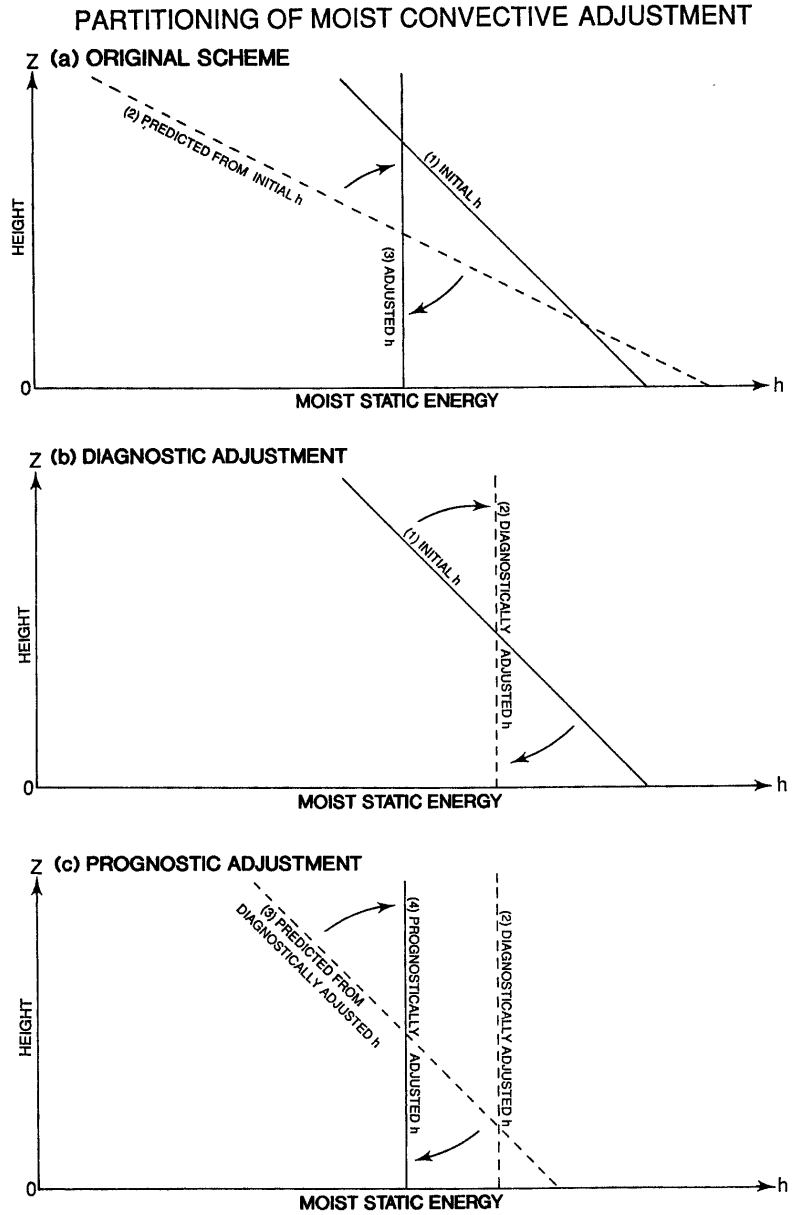

Fig. 2. Schematic of the partitioning of (a) the original scheme of moist convective adjustment into two consecutive processes of (b) diagnostic and (c) prognostic adjustments.

$$\tilde{\boldsymbol{P}}_a \Delta t = \boldsymbol{H}_a(t_0 + \Delta t) - [\boldsymbol{H}_a(t_0) + \tilde{\boldsymbol{F}} \Delta t]. \quad (2.13)$$

Figure 2 schematically illustrates the partitioning of the original MCA scheme (2.10) at time $t_0 + \Delta t$ into two consecutive processes of diagnostic (2.12a) and prognostic (2.13) adjustments. The original scheme (Fig. 2a), following the sequentially labeled steps (1), (2), and (3), temporarily predicts $\hat{h}(t_0 + \Delta t)$ from the non-adjusted initial value $h(t_0)$, and then adjusts the predicted value to $h_a(t_0 + \Delta t)$. The diagnostic-adjustment process (Fig. 2b), following steps (1) and (2), "diagnostically" adjusts $h(t_0)$ to $h_a(t_0)$. Subsequently, the prognostic-adjustment process (Fig. 2c), following steps (2), (3), and (4), temporarily predicts $\hat{h}(t_0 + \Delta t)$ from the diagnostically adjusted $h_a(t_0)$ and then "prognostically" adjusts the predicated value to $h_a(t_0 + \Delta t)$.

As schematically illustrated in Fig. 3 in the original MCA scheme (upper panel), the initial adjustment of the lapse rate at the first onset of saturation at time $t_0 + \Delta t$ is essentially through the diagnostic-adjustment process and only partly through the prognostic-adjustment process. The adjustment process after the initial adjustment is entirely through the prognostic adjustment process. In the partitioned scheme (lower panel), the initial adjustment process at $t_0 + \Delta t$ is partitioned into two consecutive processes of diagnostic and prognostic adjustments, thereby isolating diagnostic adjustment.

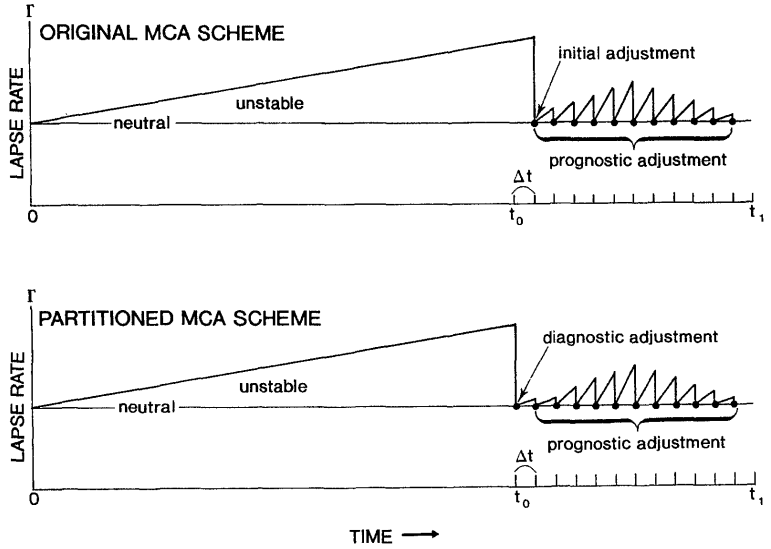

Fig. 3. Schematic of the original (upper) and partitioned (lower) schemes of moist convective adjustment. The lapse rate at a given level is plotted as a function of time. The onset of saturation is denoted by t_0, while the time increments (Δt) of MCA are indicated by tic marks. The adjusted values are indicated by solid circles.

Once diagnostic adjustment occurs at t_0, it does not occur again at $t_0 + \Delta t$, since $h(t_0 + \Delta t)$ has already been adjusted. On the other hand, prognostic adjustment occurs at $t_0 + \Delta t$, provided the conditions given by (2.5) and (2.6) are satisfied for conditional instability and thus the occurrence of MCA. If these conditions are not satisfied, MCA is interrupted, allowing conditionally unstable stratification to rebuild. Thus, diagnostic adjustment occurs intermittently, while the prognostic adjustment occurs continually as Δt approaches zero.

In the partitioned scheme, diagnostic adjustment occurs at time t_0, whereas the original MCA occurs at time $t + \Delta t_0$. When $\tilde{F}$ in (2.13) is replaced by diagnostically adjusted $\tilde{F}$, the sum of the diagnostic (2.12a) and prognostic (2.13) adjustments does not exactly equal the unpartitioned adjustment (2.10). The discrepancy, however, is negligible compared to the diagnostic adjustment that dominates prognostic adjustment. Moreover, there is no discrepancy after $t_0 + \Delta t$, since no diagnostic adjustment occurs.

2.3 The continuous scheme of MCA

At the limit of zero Δt, the discrete scheme of MCA is reduced to the continuous scheme as

$$\frac{\partial \boldsymbol{H}}{\partial t} - \boldsymbol{F} = \boldsymbol{D}_a + \boldsymbol{P}_a. \tag{2.14}$$

Here, $\boldsymbol{D}_a$ is given by the continuous form of (2.12a) and (2.12b) as

$$\boldsymbol{D}_a = \lim_{\Delta t \to 0} \frac{\boldsymbol{H}_a(t) - \boldsymbol{H}(t)}{\Delta t}, \tag{2.15a}$$

$$= [\boldsymbol{H}_a - \boldsymbol{H}]\delta(t - t_0), \tag{2.15b}$$

where $\delta(t)$ is a delta function which vanishes except at $t = t_0$.

On the other hand, $\boldsymbol{P}_a$ is given by (2.13) as

$$\boldsymbol{P}_a = \frac{\partial \boldsymbol{H}_a}{\partial t} - \boldsymbol{F}. \tag{2.16}$$

2.4 The determination of the partitioned scheme

The diagnostic- and prognostic-adjustment schemes can be explicitly determined in terms of large-scale variables, as given by (B10a,b) and (B7a,b), respectively, in Appendix B.

The explicit diagnostic-adjustment scheme (B10a,b) is simplified by replacing γ and $e(-z)$ defined by (B3b) and (B6c) with $\langle\gamma\rangle$ and $\langle e(-z)\rangle$, respectively, as

$$\tilde{D}_T \Delta t = \frac{1}{1 + \langle\gamma\rangle}[\langle h\rangle - h], \tag{2.17a}$$

and

$$\tilde{D}_q \Delta t = \frac{\langle\gamma\rangle}{1 + \langle\gamma\rangle}[\langle h\rangle - h], \tag{2.17b}$$

where

$$\gamma = \frac{L}{C_p} \cdot \frac{\partial q^*}{\partial T}. \tag{2.18}$$

Similarly, the explicit prognostic-adjustment scheme (B7a,b) is simplified as

$$P_T = \frac{1}{1 + \langle\gamma\rangle}\langle F_T + F_q\rangle - F_T, \tag{2.19a}$$

and

$$P_q = \frac{\langle\gamma\rangle}{1 + \langle\gamma\rangle}\langle F_T + F_q\rangle - F_q. \tag{2.19b}$$

2.5 Convective cancellation

In particular, when F_T and F_q consist only of vertical advection and vertical diffusion, the temperature equation with prognostic adjustment is explicitly written by use of (2.19a) as

$$C_p\frac{\partial T}{\partial t}+(S_T w-C_pV_T)$$
$$=\frac{1}{1+\langle\gamma\rangle}\left(-\langle\frac{\partial h_a}{\partial z}w\rangle+\langle C_pV_T+LV_q\rangle\right)$$
$$+(S_T w-C_pV_T), \tag{2.20}$$

where S_T is defined by

$$S_T=\frac{\partial(C_pT+\phi)}{\partial z}. \tag{2.21}$$

Here, the terms on the right-hand side of (2.20) are due only to prognostic adjustment. The V_T and V_q are the vertical diffusion of dry static energy and moisture, respectively.

Since (2.20) included identical terms on both sides, it can be reduced to

$$C_p\frac{\partial T}{\partial t}$$
$$=\frac{1}{1+\langle\gamma\rangle}\left(-\langle\frac{\partial h_a}{\partial z}w\rangle+\langle C_pV_T+LV_q\rangle\right). \tag{2.22}$$

This equation is equivalent to those derived in a different manner by Arakawa and Chen (1987, Eq. 14) and Arakawa (1993, Eq. 1.29) by assuming that MCA consists only of prognostic adjustment. It is also analogous to those derived on the basis of the convective-neutrality hypothesis by Emanuel (1987, Eq. 21), Emanuel *et al.* (1994, Eq. 37), and Brown and Bretherton (1995, Eq. 31), when the latter schemes are vertically averaged.

Since the vertical derivative of h_a vanishes owing to the MCA neutralization process, the net warming (2.22) vanishes in the absence of surface fluxes. This means that, in the absence of surface fluxes, the adiabatic cooling and vertical diffusion on the left-hand side of the temperature equation (2.20) are exactly cancelled by the terms on the right-hand side due to prognostic adjustment. It can be shown that this conclusion holds, even when the explicit scheme of prognostic adjustment (B7a) has not been simplified. This conclusion essentially follows from the assumption of a conditionally neutral and saturated atmosphere. The concept of convective cancellation based on the MCA hypothesis is analogous to that based on the convective-neutrality hypothesis (Emanuel, 1987). In spite of convective cancellation, however, horizontal and vertical velocities can change in the presence of any pressure contrast between convective and non-convective regions.

2.6 Comparison with other schemes

The partitioned MCA schemes should be equivalent to the Betts-Miller (1986) scheme in the limit of an infinitesimal time scale of relaxation, although the two schemes differ in form. The partitioned scheme is easier to interpret than the Betts-Miller scheme, since the prognostic-adjustment scheme is explicitly expressed in terms of large-scale forcing.

The heating due to prognostic adjustment is not only related to moisture convergence and evaporation, but also to adiabatic cooling and the surface flux of sensible heat. This heating is mathematically equivalent, upon convective-layer average, to that parameterized by Emanuel (1987) on the basis of the convective-neutrality hypothesis, if the large-scale moisture is assumed to be saturated for the latter heating. The two forms of heating differ from that due to the Kuo (1965, 1974) scheme which is related to moisture convergence and evaporation, as well as to the temperature difference between clouds and the environment.

The diagnostic-adjustment process neutralizes any pre-existing unstable stratification, while the prognostic-adjustment process maintains the neutralized stratification. In this respect, the two processes are formally analogous to the "initial" and "quasi-equilibrium" adjustment processes in the generalized Arakawa-Schubert scheme (Arakawa and Xu, 1992; Randall and Pan, 1993). This scheme allows the cloud mass flux to reduce any initially large value of cloud-buoyancy work and to maintain it at its quasi-equilibrium value. In contrast to the MCA scheme, however, the initial-adjustment process does not occur repeatedly. This is because the Arakawa-Schubert scheme is not turned off, even when the relative humidity becomes less than a critical value independent of the static stability.

In the linearized Betts-Miller scheme theoretically studied by Neelin and Yu (1994), the effect of diagnostic adjustment can be represented by "fast modes" which quickly decay with time. When slow and fast modes initially cancel each other and the fast modes decay, the sum of these modes grow through the transient nonmodal growth mechanism (see Farrell, 1989; Farrell and Iaonnou, 1996a,b; Trefethen *et al.*, 1993).

The moist convective-relaxation scheme of Betts and Miller (1986) was simplified (Goswami and Rao, 1994; Goswami and Mathew, 1994) by externally specifying the time-independent "equilibrium moisture", instead of internally determining quasi-equilibrium moisture as a function of time. Although this scheme appears to give some good results, the validity of this approach is questionable.

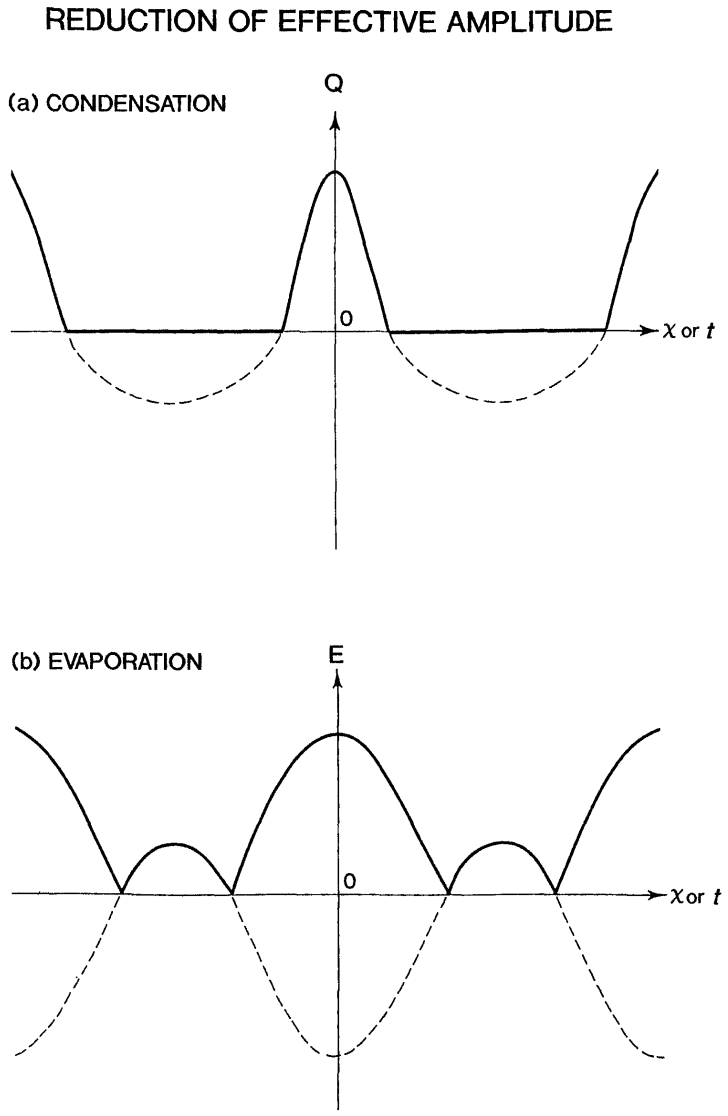

Fig. 4. Schematic of the reduction of the effective amplitudes. (a) Solid curves indicate condensation, while dashed curves indicate negative condensation which is set to zero for conditional (positive-only) heating. The alternating positive and zero values results in a reduced effective amplitude. (b) Solid curves indicate evaporation, while dashed curves indicate negative evaporation which is set to its absolute value in the nonlinear evaporation scheme. The absolute values of alternating positive and negative values result in a reduced effective amplitude.

3. Evaporation-wind feedback instability theory

3.1 The quasi-linear model

In this section, evaporation-wind feedback instability is examined by use of a theoretical Kelvin-wave model that incorporates only the prognostic-adjustment scheme in the linearized perturbation equations, thereby excluding the saturation-triggering mechanism. It is assumed that the basic state in the convective layer is conditionally neutral and saturated as a result of both diagnostic- and prognostic-adjustment processes.

Since unconditional heating is unrealistic, the effect of conditional heating is incorporated in a crude manner by assuming that the amplitude of convective heating is reduced by a certain factor. As schematically illustrated in Fig. 4a, the conditional heating only allows positive condensational heating (solid curve), while negative condensational heating is set to zero. The alternating positive and zero values of convective heating result in a reduced effective amplitude of the condensational heating.

On the other hand, surface evaporation $\boldsymbol{E}$ is parameterized as

$$E = \rho c_D |V| (q^* - q_s), \tag{3.1a}$$

where $|V|$ is the wind speed defined by

$$|V| = (u^2 + v^2)^{1/2}. \tag{3.1b}$$

The nonlinear equation (3.1a) can be linearized following Neelin *et al.* (1987) and Emanuel (1987) as

$$E' = -A^*[u']_{z=0}, \tag{3.1c}$$

where A^* is the coefficient of the linearized evaporation-wind feedback. This coefficient can be interpreted as including the additional effect of feedback between the wind and the sensible-heat flux at the surface.

To crudely incorporate the effect of nonlinear evaporation-wind feedback, it is assumed that the value of the linear feedback coefficient is reduced when the basic surface flow is not much stronger than the surface wind perturbations. As schematically illustrated in Fig. 4b, evaporation (solid curve) is proportional to the absolute value of wind velocity. The absolute value of alternating positive and negative wind velocity results in a reduced effective amplitude of the evaporation.

3.2 Governing equations

In the present paper, only Kelvin modes are examined, since the governing equations can be drastically simplified for Kelvin modes, which have no meridional component in the absence of wind shear and frictional convergence. The simplified equations are mathematically equivalent to those for two-dimensional irrotational gravity waves in the zonal-vertical domain.

The present model does not allow for a subcloud layer. The effects of the basic flow are neglected, except in the parameterized surface flux of latent and sensible heat. Frictional and radiative cooling processes are also neglected.

The linearized equations with the Boussinesq approximation in log-pressure coordinates are given by

$$\frac{\partial u'}{\partial t} = -\frac{\partial \phi'}{\partial x}, \tag{3.2a}$$

$$\frac{\partial T'}{\partial t} + \frac{H}{R}\overline{S}w' = \frac{1}{C_p}P'_T, \tag{3.2b}$$

$$\frac{\partial \phi'}{\partial z} = \frac{R}{H}T', \tag{3.2c}$$

and

$$\frac{\partial u'}{\partial x} + \frac{\partial w'}{\partial z} = 0, \tag{3.2d}$$

where $\overline{S}$ is the buoyancy frequency squared, given by

$$\overline{S} = \frac{R}{C_p H}\overline{S}_T. \tag{3.2e}$$

In (3.2b), P'_T is the linearized prognostic-adjustment heating resulting from adiabatic cooling, vertical moisture advection, and evaporation-wind feedback. It is given by (2.20) as

$$P'_T = \varepsilon\left(\frac{C_p H}{R}\overline{S}w' + \frac{1}{1+\langle\gamma\rangle}\cdot\frac{L}{\rho_0 z_T}\cdot E'\right). \tag{3.3}$$

Here, ε is an amplitude reduction factor resulting from conditional heating, while z_T is the height of the convective layer.

Eliminating variables from the linearized equations and assuming a solution in the form $\exp(ikx - i\sigma t)$ results in the vertical structure equation given by

$$c^2\frac{\partial^2 w'}{\partial z^2} + \overline{S}w' = \frac{R}{C_p H}P'_T, \tag{3.4}$$

where

$$c^2 = \sigma^2/k^2. \tag{3.5}$$

Here, c is the complex phase speed, σ the complex frequency, and k the zonal wavenumber.

Inserting (3.3) into (3.4) with (3.1b) and (3.2d) results in

$$c^2\frac{\partial^2 w'}{\partial z^2} + \overline{S}_e w' = -i\frac{RA_e}{H(1+\langle\gamma\rangle)k}\left[\frac{\partial w'}{\partial z}\right]_{z=0}, \quad \text{for } 0 \le z \le z_T, \tag{3.6a}$$

and

$$c^2\frac{\partial^2 w'}{\partial z^2} + \overline{S}w' = 0, \text{ for } z \ge z_T. \tag{3.6b}$$

Here, $\overline{S}_e$ and A_e are the effective static stability and effective evaporation-wind feedback coefficients, respectively, defined by

$$\overline{S}_e = (1-\varepsilon)\overline{S}, \tag{3.7a}$$

and

$$A_e = \frac{L}{\rho z_T C_p}\varepsilon A^*. \tag{3.7b}$$

The effective static stability crudely incorporates the effect of conditional heating. It differs from the conventional "moist-reduced static stability ($\partial h^*/\partial z$)". It also differs from the "gross moist stability (Δm)" defined by Neelin and Held (1987).

The effective evaporation-wind feedback coefficient crudely incorporates the nonlinear feedback by replacing A^* in (3.7b) with a smaller value than the linear feedback coefficient to crudely incorporate the nonlinear effect.

In the present model, $\langle\gamma\rangle$ is set to 1.0, since the value of γ observationally varies with height from 0.0 to 3.0 in the tropical troposphere (see Arakawa and Schubert, 1974, Fig. 7; Bates *et al.*, 1978, Fig. 1). In the present model, the boundary layer is not incorporated, although it is more realistic to incorporate a well-mixed layer in which S_T, Q_T, and Q_q vanish.

3.3 The two-layer model

In order to compare the present model with conventional two-layer evaporation-wind feedback models, a two-layer model is first examined.

The finite difference form of (3.6a) for a two-layer model is given by

$$-c^2\frac{2w'}{(\Delta z)^2}+\overline{S}_e w'=-i\frac{RA_e}{H(1+\langle\gamma\rangle)k}\cdot\frac{w'}{\Delta z}, \qquad (3.8)$$

where Δ_z is the vertical increment which equals $z_T/2$.

This model has three levels for w, which is assumed to vanish at the bottom and top of the convective layer. Except for the absence of friction, Newtonian cooling, and zonal advection, this model is mathematically equivalent to the two-layer linear model of Neelin *et al.* (1987), in which $\langle\gamma\rangle$ was set to zero and the moist-reduced static stability was used in order to crudely parameterize cumulus heating. The equivalence between the two models is, however, limited to the two-layer model. In the present model, the effective static stability results from linearizing conditional heating, while the moist-reduced stability in their model results from the large-scale condensation process. The present two-layer model is mathematically analogous to that of Emanuel (1987) based on the convective-neutrality hypothesis.

The resulting eigenvalue σ is given by

$$\sigma^2=c_0^2k^2+ikA, \qquad (3.9a)$$

where

$$c_0^2=\overline{S}_e(\Delta z)^2/2, \qquad (3.9b)$$

and

$$A=\frac{R}{\rho(1+\langle\gamma\rangle)H}\cdot\frac{L}{C_p}\cdot\frac{\Delta z}{z_T}\varepsilon A^*. \qquad (3.9c)$$

Here, a positive value of R_e (6) corresponds to that of the eastward-moving Kelvin mode on a beta plane. When $\varepsilon=1$ in (3.3) and $\langle\gamma\rangle=0$ in (3.9c), the eigenvalue (3.9a) is equivalent to Eq. (13) of Neelin *et al.* (1987) with B in their equations redefined as $B=(R/2)(\Delta p/p)$. When $\Delta p=p=500$ m, this B is reduced to $R/2$, as it was originally defined.

When $c_0=0$, (3.9a) is reduced (see Lau and Shen, 1988, Eq. 19) to

$$\sigma=\pm(1+i)\left(\frac{kA}{2}\right)^{1/2}. \qquad (3.9d)$$

3.4 The five-layer model

Since the two-layer model excludes the 25–30-day TIO and 10–20-day Kelvin wave associated with higher vertical modes, a five-layer model is examined.

Figure 5 schematically illustrates the levels of the five-layer model. This model has six levels for w, which is assumed to vanish at level 0 (0 km) and level 5 (20 km). The prognostic-adjustment heating is assumed to vanish above z_T (10 km). The finite-difference forms of (3.6a) and (3.6b) can be found in Appendix C.

The eigenvalue equation is derived in Appendix C as

$$B_4\lambda^4+B_3\lambda^3+B_2\lambda^2+B_1\lambda+B_0=0, \qquad (3.10a)$$

where λ is the eigenvalue defined by

$$\lambda=\left(\frac{\sigma}{k\Delta z}\right)^2, \qquad (3.10b)$$

and the coefficients of (3.10a) are functions of $\overline{S}_e$ and A_e.

The period and e-folding time are determined by the real and imaginary parts of σ as $2\pi/Re(\sigma)$ and $1/Im(\sigma)$, respectively.

The effective static stabilities $\overline{S}_1$ and $\overline{S}_2$ at level 1 (2.5 km) and level 2 (7.5 km) are chosen to be $\overline{S}_1=\overline{S}_2=0.05$ N^2 in order to obtain the 40–50-day mode, where N has a typical value of tropospheric buoyancy frequency (10^{-2} s^{-1}). The static stability $\overline{S}_3$ at level 3 (12.5 km) is $\overline{S}_3=0.5$ N^2, while $\overline{S}_4=1.0$ N^2 at level 4 (17.5 km). The lid placed at 20 km can be interpreted as crudely incorporating the effect of a very stable stratosphere. The effective evaporation-wind feedback coefficient A_e is $A_e=0.04$ (K/day) (m/s)$^{-1}$, being close to the typical effective value (0.05) suggested by Neelin *et al.* (1987) on the basis of E' and u' estimated form a simulated TIO. It is assumed that the basic wind is easterly (*i.e.*, A^* is a positive coefficient). An easterly basic wind is crucial for eastward-moving waves to grow through linear evaporation-wind feedback instability (Neelin *et al.*, 1987; Emanuel, 1987).

3.5 Frequency and growth rate

Four vertical eigenmodes (H,I,J,K) can be obtained from the five-layer model. Of these four modes, Mode H is the highest vertical model, and Mode K the lowest. Mode H is almost stationary and neutral for plausible values of the parameters. Modes I,J, and K are non-stationary and unstable, corresponding to the 40–50-day TIO, the 25–30-day TIO, and the 10–20-day Kelvin wave, respectively. Mode I corresponds to the TIO mode of Neelin *et al.* (1987), Emanuel (1987), and Neelin an Yu (1994).

Figure 6a shows the linear frequencies (left) and logarithmic growth rates (right) of the Kelvin modes as functions of zonal wavenumber for Modes I (thick solid line), J (thin solid line), and K (dashed line). The respective periods of these modes for wavenumber one are 42.1, 27.2, and 15.9 days. It can be seen that the frequencies of all these modes increase with wavenumber, while the growth rates increase only slightly over wavenumbers 1–5, leveling off at higher wavenumbers. Mode I is strongly unstable with an

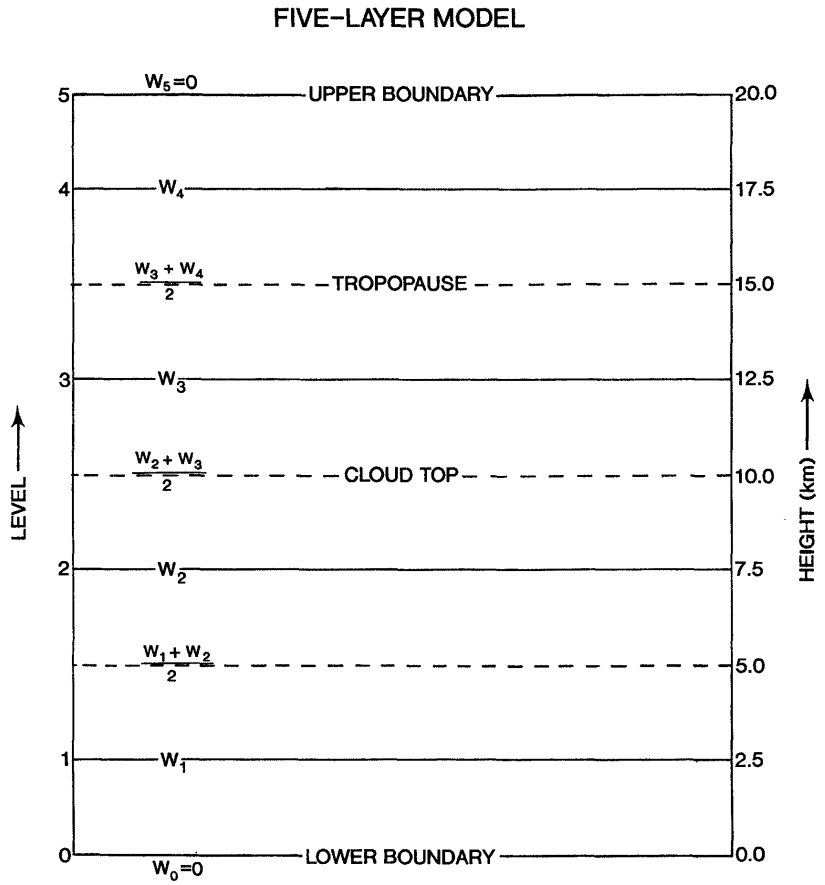

Fig. 5. Schematic of the five-layer finite-difference model with six levels.

e-folding times of less than 10 days, while Modes J and K are both weakly unstable with e-folding times greater than 100 days. The phase velocities are represented by the slopes of the wavenumber-frequency curves in the left panel. The slope for Mode I decreases with wavenumber, while the slopes for Modes J and K are almost constant.

Mode I is sensitive to the effective values of the evaporation-wind feedback coefficient and static stability. The phase-velocity slope for Mode I in the absence of evaporation-wind feedback (Fig. 6a, dotted line) is constant, as expected from (3.9a). The phase velocities of Modes J and K are almost unchanged (not shown). Figure 6b is the same as Fig. 6a, expect that the effective static stability is set to zero (*i.e.*, no conditional heating). The frequencies and growth rates of Modes J and K are almost unaffected. In contrast, the frequency (left panel) of Mode I follows the $k^{1/2}$ curve, as expected from (3.9d), while the logarithmic growth rate (right panel) of Mode I follows the log k curve. It is seen that the frequency and growth rate of Mode I are sensitive to the effective stability except for low wavenumbers.

Figure 7a illustrates the dependence of the logarithmic frequency and logarithmic growth rate of the wavenumber-one Kelvin waves on the effective evaporation-wind feedback coefficient A_e. It is seen that the frequency of Mode I increases substantially with A_e, the period shortening from 70.2 to 27.0 days as A_e increases from 0.0 to $1.0 \times A_0$, where $A_0 = 0.1$ K/day/ms^{-1}. In contrast, the frequencies of Modes J and K hardly change with A_e. It turns out that the frequency of Mode I coincides with that of J near a value of $A_e = 1.0 \times A_0$ and exceeds it (not illustrated) for larger values. All these modes have a zero growth rate at $A_e = 0.0$, in contrast to wave-CISK theory (Hayashi, 1970). The growth rate of Mode I increases substantially with A_e, the e-folding time shortening from infinity to 5.4 days as the value of A_e increases from 0.0 to $1.0 \times A_0$. Modes J and K exhibit much smaller growth rates than Mode I for these values of A_e.

Figure 7b illustrates the dependence of the logarithmic frequency and logarithmic growth rates of the wavenumber-one Kelvin waves on the effective static stability $\overline{S}_e$ at level 1 and 2. It is seen that the frequency of Mode I increses substantially with $\overline{S}_e$, the period shortening from 46.5 to 24.2 days as $\overline{S}_e$ increases from 0.0 to $1.0 \times (\mathrm{N}^2)$. In contrast, the frequencies of Modes J and K exhibit only moderate increases. The growth rate of Mode I decreases substantially with $\overline{S}_e$, whereas those of Modes J

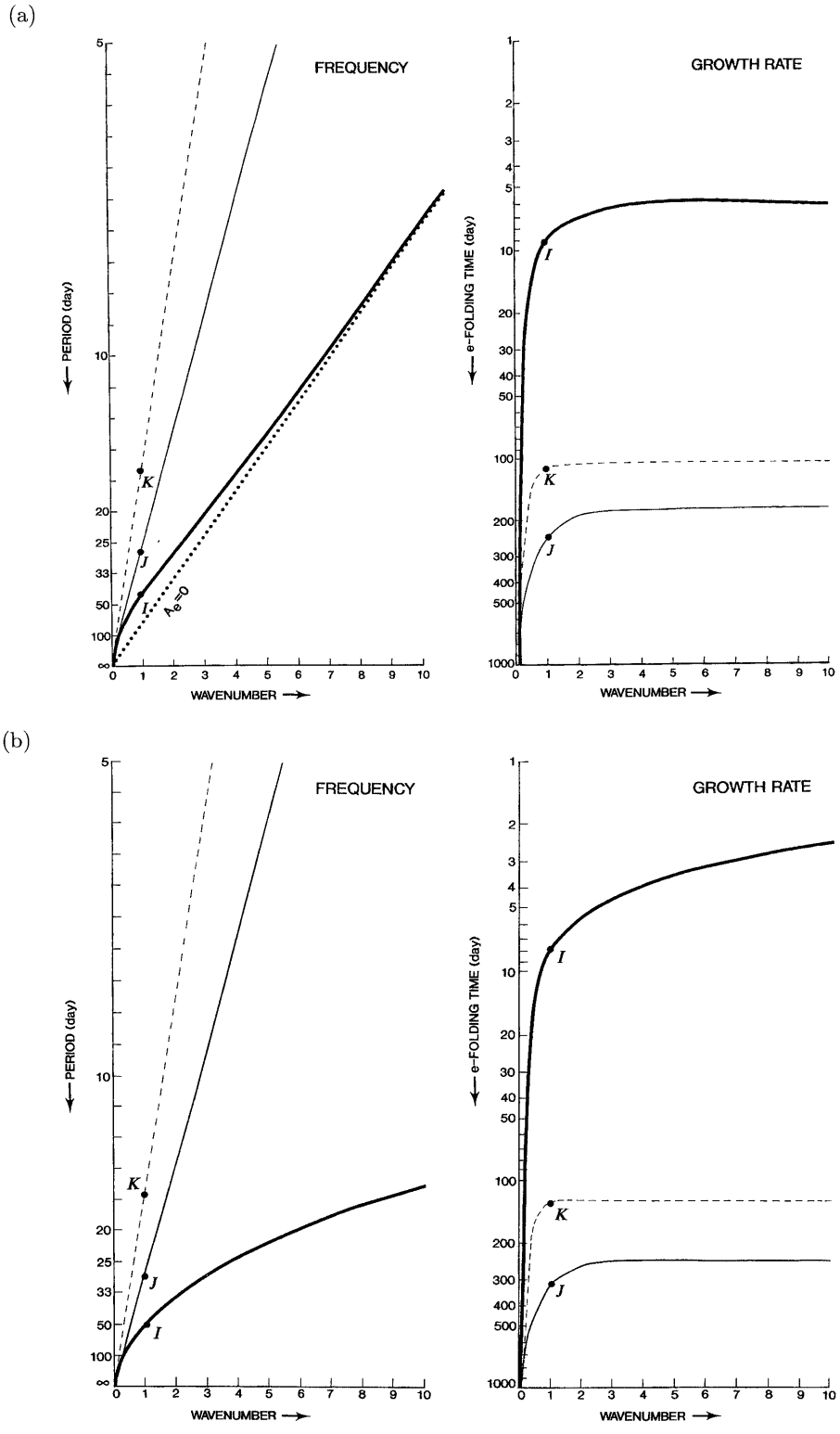

Fig. 6. (a) Linear frequencies (left) and logarithmic growth rates (right) of Kelvin waves for Mode I (thick solid line), Mode J (thin solid line), and Mode K (thin dashed line) of the five-layer model as functions of zonal wavenumber. The effective static stability $\overline{S}_e$ in the lowest two layers is 0.05 N^2, while the effective evaporation-wind feedback coefficient A_e is 0.04 K/day/(ms^{-1}). Solid circles on the lines indicate eigenvalues for wavenumber one. In addition to the three lines, the dotted line indicates the frequency of Mode I when A_e is set to zero. The frequencies of Modes J and K for $A_e = 0$ are not indicated, since these values are almost unchanged. (b) As in Fig. 5a, except that S_e is set to zero, while A_e is kept at 0.4 A_0.

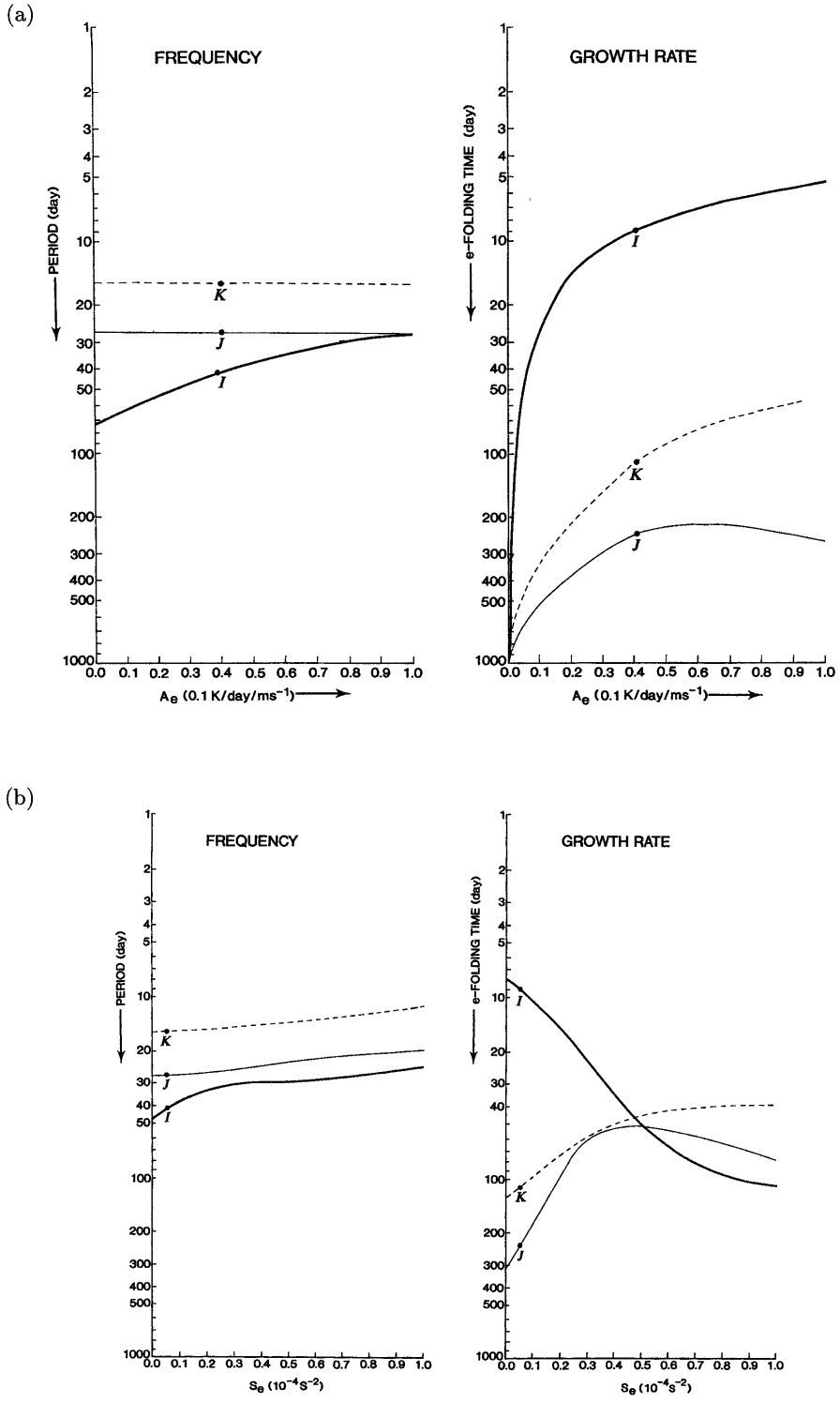

Fig. 7. (a) Logarithmic frequencies (left) and logarithmic growth rates (right) of wavenumber-one Kelvin waves for Mode I (thick solid line), Mode J (thin solid line), and Mode K (thin dashed line) of the five-layer model as functions of A_e. The value of $\overline{S}_e$ is fixed at the same value as used in Fig. 6a. Solid circles on the lines indicate eigenvalues for the same value of A_e as used in Fig. 6a. (b) As in Fig. 7a, except that the logarithmic frequencies and growth rates are plotted as functions $\overline{S}_e$. The value of A_e is fixed at the same value as used in Fig. 6a. Solid circles on the lines indicate eigenvalues for the same value of $\overline{S}_e$ as used in Fig. 6a

Table 1a

	Mode I	Mode J	Mode K
Periods (days)	42.1	27.2	15.9
e-folding times (days)	9.2	239.0	111.1
vertical wavelength (km)	5.30	5.34	9.18
vertical decay scale (km)	1.1	46.9	64.4

Table 1b

	Mode I	Mode J	Mode K
periods (days)	42.1	27.2	15.9
e-folding times (days)	∞	∞	∞
vertical wavelength (km)	3.45	5.34	9.18
vertical decay scale (km)	∞	∞	∞

Table 1c

	Mode I	Mode J	Mode K
periods (days)	42.1	27.2	15.9
e-folding times (days)	10.1	10.0	10.0
vertical wavelength (km)	5.00	6.35	9.76
vertical decay scale (km)	1.2	2.3	6.2

and K increase substantially with $\overline{S}_e$ for $\overline{S}_e \langle 0.5\ \mathrm{N}^2$. The three modes have similar growth rates (e-folding times of about 50 days) for $\overline{S}_e = 0.5\ \mathrm{N}^2$.

For $\overline{S}_e = 0$ and $A_e = 0$ (not illustrated), the growth rates of Modes H,I,J, and K are zero, with their wavenumber-one periods being $^\infty$,$^\infty$, 27.2, and 15.9 days, respectively. The non-zero frequencies of Modes J and K are not contrary to convective cancellation since the temperatures (*i.e.*, vertical derivative of geopotential height) of these modes vanish in the convective layer, although the geopotential height changes with time.

3.6 Vertical wavelength and vertical decaying scale

Since the vertical structures of Modes I,J,K in the troposphere are determined essentially by convective heating, these modes are similar to the baroclinic mode in the two-layer model in that the zonal velocity reverses its sign between the lower- and upper-tropospheric levels, with maximum vertical velocity occurring at the mid-tropospheric level. Above the level of convective heating, however, their vertical structures are determined by their frequencies and growth rates through the dispersion relation given by

$$m^2 = \overline{S}k^2/\sigma^2, \tag{3.11}$$

where m is the complex vertical wavenumber.

The vertical wavelength and e-folding vertical decay scale are determined by the real and imaginary parts of m as $2\pi/Re(m)$ and $1/Im(m)$, respectively.

Table 1a lists the vertical wavelengths and decay lengths of Mode I,J,K for zonal wavenumber one and for a buoyancy frequency (square root of $\overline{S}$) of 0.02 s^{-1}, which is a typical value observed in the stratosphere. It is seen that the vertical wavelengths of Mode I and J are comparable ($\sim$ 5 km), while that of Mode K is twice as large. Mode I has a much smaller vertical decay scale ($\sim$ 1 km) than Mode J and K ($\sim$ 50 km), implying that the energy of Mode I is confined to the troposphere, while those of Mode J and K hardly decay with height in the stratosphere. This result means that the stronger the vertical convergence of energy, the stronger the growth rate.

Since the growth rate not only determines the vertical scale but also affects the vertical wavelength of low-frequency waves, Table 1b shows the results when the growth rates are set to zero (*i.e.*, infinite e-folding time) for the three modes. It is seen that the vertical wavelength of Mode I is reduced to 3.4, while those of Mode J and K are hardly affected. On the other hand, the vertical decay scales become infinite for all three modes, implying that these modes have no vertical convergence of kinetic energy when they do not grow.

Since the growth rates of Mode J and K could be greatly enhanced by fully incorporating nonlinear effects, the e-folding time of Modes I,J,K are set to 10.0 days in Table 1c to increase the growth rates of Mode J and K by an order of magnitude. It is seen that the vertical wavelengths are hardly affected, while the vertical decay scales of Modes J and K are reduced by an order of magnitude.

4. Interpretations of the results

The present results indicate that within the range of plausible values for the effective static stability and the EWF coefficient, the growth rates for wavenumber-one Mode J and K are too small for

these modes to grow in the presence of Newtonian cooling having a damping time of 10–20 days. In order to explain the observed and simulated 25–30-day TIO and 10–20-day Kelvin wave, the full nonlinear effects of conditional heating and/or the ST mechanism must be incorporated.

The slow phase speed of the 40–50-day mode in the present linear model is due to the reduced value (5 %) of effective static stability. This value was chosen to obtain the 40–50-day period. The justification and determination of the real effective value should involve the consideration of the full nonlinear effects of conditional heating. The results for a zero value, however, can be interpreted as those for unconditional heating.

Although the present quasi-linear model does not explain the dominance of the wavenumber-one component of the observed and simulated TIOs, the effective static stability eliminates the preference for the higher wavenumber components. The EWF growth rates of Kelvin modes increase only slightly with wavenumber, allowing the preferred scale to be modified by the neglected effects such as horizontal diffusion, fully nonlinear conditional heating, and nonlinear advection. The dominance of the wavenumber-one TIO is found in a nonlinear EWF model that incorporates the full nonlinear effects of conditional heating (Xie *et al.*, 1993a,b).

In contrast, the growth rate of Kelvin modes due to wave-CISK increases drastically with wavenumber (Hayashi, 1970). The preferred scale of wave-CISK with fully nonlinear conditional heating depends on several factors, such as the strength and vertical distribution of the heating parameter, nonlinear advection, horizontal diffusion, and horizontal resolution (see Lau and Peng, 1987; Miyahara, 1987; Itoh, 1989; Yoshizaki, 1991; Dunkerton and Crum, 1991; Crum and Dunkerton, 1992, 1994; Xie, 1994). Frictional convergence greatly enhances the growth rate of Kelvin wave-CISK (Hayashi, 1971b; Wang, 1988). Without conditional heating, however, frictional wave-CISK does not result in the low-wavenumber dominance of Kelvin waves and TIOs (Hayashi, 1971b; Xie and Kubokawa, 1990; Ohuchi and Yamasaki, 1997).

The present model is equivalent to the linear EWF model of Neelin *et al.* (1987) based on the large-scale condensation process, and also analogous to that of Emanuel (1987) based on the convective-neutrality hypothesis. The present model, however, is based on the MCA hypothesis and conceptually differs from these models. The conditionally neutral and saturated basic state is interpreted as resulting from both the diagnostic and prognostic adjustment processes, rather than invoking the convective-neutrality hypothesis. Moreover, the EWF mechanism examined here is part of the united mechanisms. The present multilayer model allows for more vertical modes than the other tropospheric models.

The present model is equivalent to the linear EWF model of Neelin and Yu (1994) using the Betts-Miller scheme, except that the present model explicitly expresses the prognostic-adjustment process in terms of large-scale forcing. Their model allows "propagating deep convective mode" that corresponds to Mode I, but does not allow Modes J and K, since their model has either a lid or radiation condition at the top of the convective layer. In a model with realistic stratification, Mode I essentially depends on the partial reflection around the top of the convective layer, while Modes J and K essentially depend on that around the tropopause. The lid condition imposed in the present model can be interpreted as crudely incorporating the partial reflection around the tropopause due to the strong vertical gradient of the static stability.

More realistically, when the lid is placed at an infinite height, the eigenvalues become continuous (Hayashi, 1976; Cohn and Dee, 1989). When all the eigenmodes are integrated over the continuous eigenvalues, these modes should be consistent with an open boundary condition. Also, there should be several preferred unstable modes among the continuous eigenmodes that have relatively strong growth rates resulting from several levels of relatively strong reflection. There should also be several preferred quasi-resonant modes that have a relatively strong resonant response resulting from relatively strong partial reflection (see Gill 1982, p. 287). The partial reflection at the tropopause is enhanced by moist-reduced tropospheric stability. The resonance due to partial reflection will reinforce the "non-singular" resonance (Hayashi, 1976) that occurs when the vertical scale of waves matches the characteristic vertical scales of the thermal forcing. In a model with realistic stratification and realistic vertical distribution of convective heating, both partial-reflection and non-singular resonances will occur.

In the absence of convective heating, there are no free internal modes except for an external free mode under the radiation condition (Lindzed, 1967). There are only discrete eigenvalues in wave-CISK theory (Hayashi, 1971a) and evaporation-wind feedback theory (Neelin and Yu, 1994) under the radiation condition. The radiation condition as directly applied to individual eigenmodes, however, is appropriate only for unstable modes, since it eliminates continuous free modes. Incorporating the effect of the reflection around the stratopause in the present model allows for Mode L, which would correspond to the observed (Hirota, 1978) and simulated (Hayashi *et al.*, 1984) and simulated (Hayashi *et al.*, 1984) mesospheric upper-stratospheric 5–7-day Kelvin waves. Incoporating the effect of reflection around the mesopause also allows for Mode M, which would correspond to the observed (Salby *et*

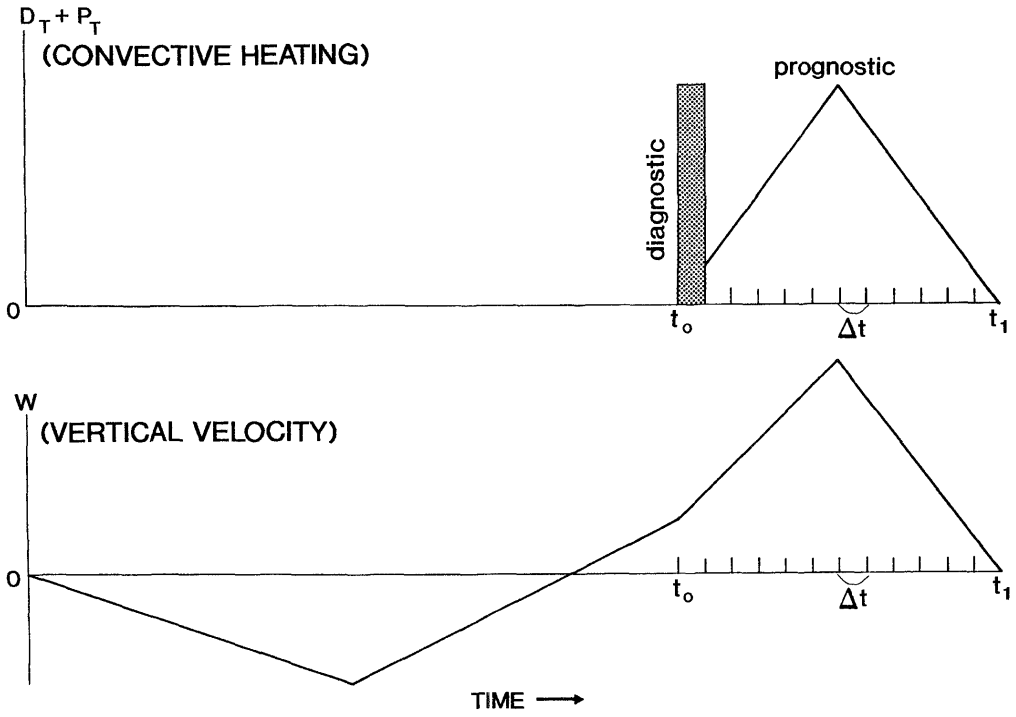

Fig. 8. Schematic of the original scheme of moist convective adjustment. MCA heating (upper panel) and vertical velocity (lower panel) at the mid-tropospheric level.

al., 1984) 3–4-day Kelvin waves.

5. Interpretations of the saturation-triggering mechanism

This section dynamically interprets the saturation-triggering mechanism in terms of the partitioned MCA processes.

5.1 Diagnostic- and prognostic-adjustment processes

Diagnostic adjustment represents the ensemble effect of rapidly growing non-equilibrium moist convection. This process restores convective equilibrium and is a function of temperature and moisture. As schematically illustrated in Fig. 8, it does not directly depend on large-scale vertical velocity, but its magnitude depends on the large-scale temperature and moisture fields while its occurrence depends on saturation. As will be described in the following subsections, diagnostic adjustment forces gravity waves, cloud clusters, and superclusters through the "non-resonant" ST mechanism, while it forces Kelvin and MRG waves through the "resonant" ST mechanism.

Prognostic adjustment represents the ensemble effect of quasi-equilibrium moist convection. This process maintains convective equilibrium and is a function of the large-scale heating and moisture terms, such as adiabatic cooling, moisture convergence, and surface evaporation. It directly depends on the large-scale vertical velocity (see Fig. 8), and reduces the effective static stability and phase velocities. Prognostic adjustment is crucial to the evaporation-wind feedback instability of TIOs.

5.2 The non-resonant saturation-triggering mechanism

The following non-resonant ST mechanism is high speculative, but has been substantiated by a detailed analysis of a high-resolution simulation of superclusters, as will be demonstrated in a subsequent paper (Numaguti and Hayashi, 1997).

When the conditionally unstable atmosphere becomes saturated at a certain point, diagnostic adjustment triggers both westward- and eastward-moving gravity-wave packets. The westward-moving packet results in condensation and forms cloud clusters. On the other hand, the eastward-moving packet causes saturation and diagnostic adjustment at a point east of the original point, again forming westward-moving cloud clusters. The eastward-moving patterns forming the envelope of westward-moving cloud clusters are interpreted as superclusters. The east-west asymmetry is due to the earth (*i.e.*, the beta effect).

5.3 The resonant saturation-triggering mechanism

In particular, Kelvin and MRG waves are interpreted as planetary waves resonantly amplified through the following resonant ST mechanism: It is assume that cloud clusters are generated through the non-resonant ST mechanism. As schematically illustrated in Fig. 9a, the intermittent occurrence

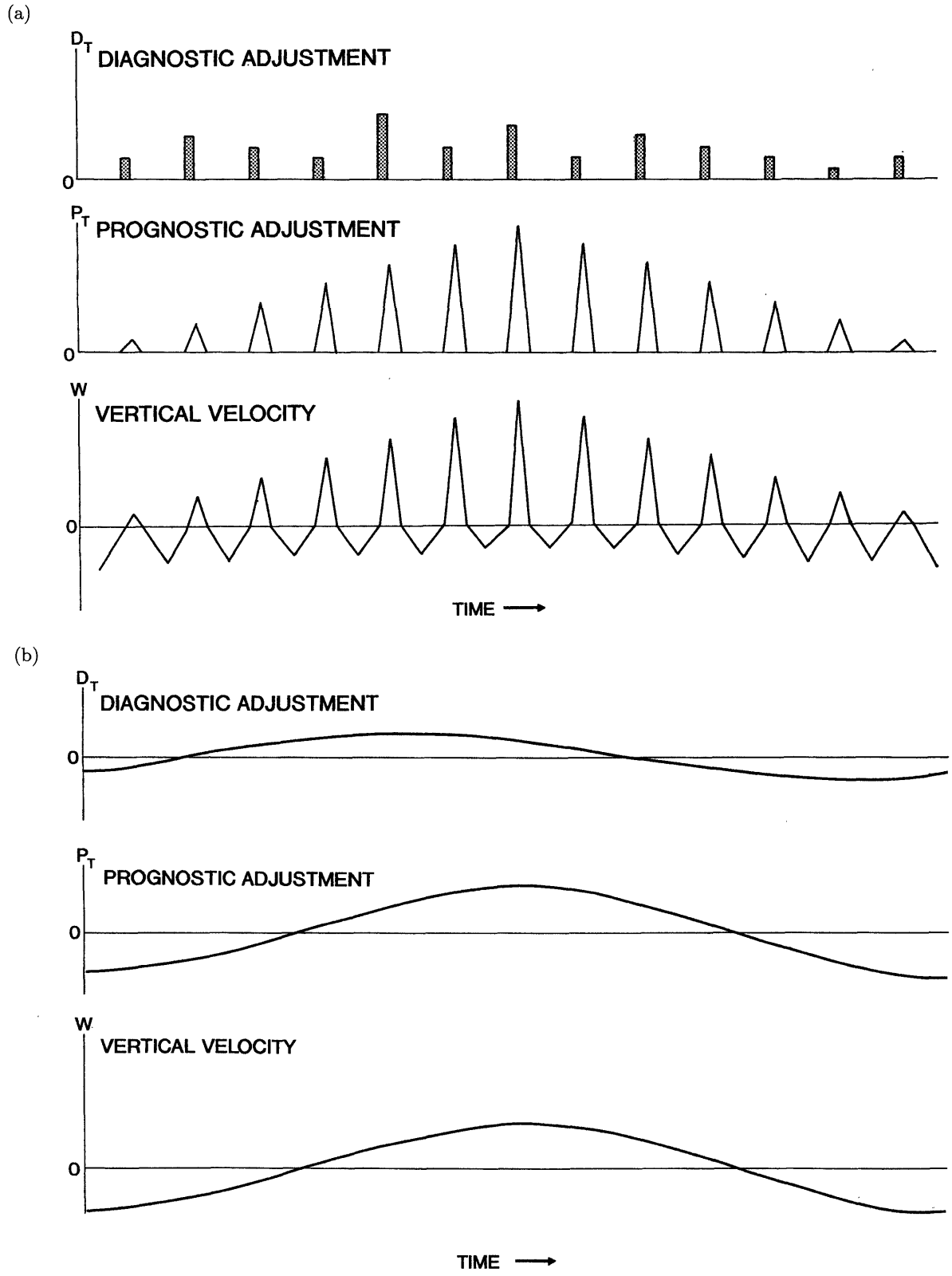

Fig. 9. (a) Schematic of the resonant saturation-triggering mechanism. Diagnostic-adjustment heating (upper), prognostic-adjustment heating (middle), and vertical velocity (lower) are plotted as functions of time. Irregular time intervals between the intermittent onset of heating are represented by equal intervals. (b) As in Fig. 9a, except for the resonant Fourier components.

of diagnostic-adjustment heating associated with cloud clusters can be regarded as random forcing of planetary-scale waves. The intermittent nature is due to the MCA process being turned off during periods of nonsaturation. The randomness results from the history of temperature and moisture involving the nonlinear process. On the other hand, the prognostic-adjustment heating associated with these waves is regarded as a feedback to the forcing, resulting in reduced values of the effective static stability.

The vertical velocity and prognostic-adjustment heating should exhibit distinct space-time scales through their resonant response to random forcing. The resonant Fourier components implicit in Fig. 9a are schematically illustrated in Fig. 9b. These components are exaggerated in both Fig. 9a and 9b in order to clearly distinguish them from random components. In practice, the noise in the spectra resulting from the random components would make it difficult to clearly detect any resonant spectral peaks in the vertical velocity and any feedback spectral peaks in the heating due to prognostic adjustment. The resonant peaks occurring in the winds, however, can be clearly detected, since the planetary-wave components of the winds dominate random gravity-wave components of the winds. In contrast to vertically propagating MRG waves, a tropospherically confined MRG wave exhibits a rather distinct periodicity in the associated precipitation (Hendon and Liebman, 1991). This periodicity could be due to a strong spectral peak in the feedback heating associated with this wave.

5.4 Implications for random thermal-forcing theory

The resonant ST mechanism is analogous to the random thermal-forcing mechanism, except that the former incorporates feedback heating such as the prognostic-adjustment process. The resonant-wave components in a random thermal-forcing model (Hayashi, 1976) are characterized by an unrealistic quadrature-phase relationship between vertical velocity and heating. This defect can be alleviated by incorporating feedback heating in random thermal-forcing theory as explained in the following.

In the presence of only adiabatic cooling and heating due to diagnostic (D_T) and prognostic (P_T) adjustments, the heat balance equation is written as

$$T_t + Sw = D_T + P_T, \tag{5.1}$$

where T_t is the temperature tendency, S the static stability, and w the vertical velocity.

In the absence of D_T, the adiabatic cooling Sw exactly balances P_T in convective regions by virtue of convective cancellation. The Fourier components of Sw, however, do not completely balance those of P_T, since P_T vanishes in nonconvective regions, resulting in a non-zero value of the effective static stability. In the presence of D_T, on the other hand, the resonant and nonresonant components have different balances.

For the non-resonant components, T_t is relatively small and Sw nearly balances $D_T + P_T$ as

$$Sw = D_T + P_T. \tag{5.2}$$

It follows that w is nearly in phase with $D_T + P_T$, while T can also be nearly in phase with $D_T + P_T$.

For the resonant components, in contrast, temperature tendency (T_t) and ($Sw - P_T$) have relatively large values and nearly cancel each other to balance the relatively small value of D_T as

$$T_t + (Sw - P_T) = D_T. \tag{5.3}$$

It turns out (Hayashi 1976) that D_T is nearly in quadrature with ($Sw - P_T$). Since Sw and P_T are nearly in phase, D_T is also nearly in quadrature with w for the resonant components. The phase relations between the resonant Fourier components of D_T,P_T, and W are schematically illustrated in Fig. 9b.

The quadrature-phase relationship between w and D_T has been considered a defect in the conventional random thermal-forcing theory, since only D_T is interpreted as thermal forcing and P_T is ignored. However, w is nearly in phase with $D_T + P_T$, even for the resonant components, since P_T is nearly in phase with w and dominates D_T, as expected from the heat balance (5.3) for the resonant components.

Itoh (1977) and Horinouchi and Yoden (1996) pointed out that localized vertical velocity, consisting of both resonant and nonresonant components, occurs near the localized heating (see Fig. 9a). In other words, the local vertical velocity can be locally non-resonant to local heating. Nevertheless, the resonant *non-local* Fourier components still have an unrealistic phase relation.

The linear response of equatorial waves to externally prescribed thermal forcing was examined by Manzini and Hamilton (1993) and Bergman and Salby (1994) with the use of numerically simulated and observed convective heating, respectively. In terms of MCA, this heating can be interpreted as the sum of D_T and P_T. On the other hand, Salby and Hendon (1994) externally imposed random heating in a linear model with wave-CISK heating to study the generation of TIOs. The random and wave-CISK heating are analogous to D_T and P_T, respectively. When feedback heating is incorporated, random thermal-forcing theory will be improved with respect to the phase relation, vertical wavelength, and phase velocity of Kelvin and MRG waves.

6. Conclusions and remarks

To theoretically interpret the united mechanisms for the generation of low- and high-frequency tropical waves, the process of moist convective adjustment (MCA) was conceptually partitioned into two

consecutive processes of "diagnostic" and "prognostic" adjustments. Diagnostic adjustment intermittently neutralizes, upon saturation, any pre-existing conditionally unstable stratification, thereby restoring convective equilibrium. Prognostic adjustment continually neutralizes, during saturation, any predicted conditionally unstable stratification, thereby maintaining the restored convective equilibrium. Diagnostic adjustment is crucial to the saturation-triggering (ST) mechanism, while prognostic adjustment is crucial to the evaporation-wind feedback (EWF) mechanism. The two processes were then mathematically determined as functions of the large-scale temperature-moisture field and large-scale forcing, respectively.

As a step toward a unified theory, EWF instability was examined by the use of a theoretical Kelvin-wave model that incorporates only the prognostic-adjustment process in the linearized perturbation equation, thereby excluding the ST mechanism. It was assumed that the basic state in the convective layer is conditionally neutral and saturated as a result of both the diagnostic- and prognostic-adjustment processes. The prognostic-adjustment process includes only temperature and moisture changes due to adiabatic cooling, vertical moisture advection, and evaporation-wind feedback. The nonlinear effects of conditional heating and evaporation wind-feedback were crudely incorporated through adjustable values of the "effective static stability" and the "effective EWF coefficient", respectively. The following conclusions were obtained.

1) In the absence of the surface flux of latent and sensible heat, prognostic-adjustment heating is exactly canceled by large-scale adiabatic cooling, vertical advection, and vertical diffusion, resulting in no change in the large-scale temperature in convective regions (*i.e.*, "MCA convective cancellation").

2) For a plausible choice of the adjustable parameters, the resulting vertical eigenmodes include one strongly unstable mode (Mode I), which corresponds to the 40–50-day TIO, and two weakly unstable modes (Modes J and K), which correspond to the 25–30-day TIO and the 10–20-day Kelvin wave, respectively.

3) The frequency of Mode I is an increasing function of the effective evaporation-wind feedback coefficient, while those of Modes J and K exhibit little change. The growth rates of the three eigenmodes are increasing functions of small values of this coefficient. In the absence of evaporation-wind feedback, these eigenmodes become neutral, consistent with the MCA convective cancellation, but in contrast to wave-CISK theory.

4) The frequencies of the three eigenmodes are increasing functions of the effective static stability. The growth rate of Mode I is a decreasing function of the effective static stability, while those of Modes J and K are increasing functions of small effective static stability.

The present results are based on the MCA scheme. Other schemes, such as those proposed by Gadd and Keers (1970), Kurihara (1973), Arakawa and Schubert (1974), Emanuel (1991), and Hack (1994) do not assume a critical value of relative humidity below which parameterized moist convection is suppressed, regardless of stratification. It follows that the other schemes do not allow the stratification to become unstable during periods of subcritical relative humidity and therefore do not allow the ST mechanism.

The present theory yields three vertical modes corresponding to the observed and simulated 40–50- and 25–30-day TIOs and 10–20-day Kelvin wave for a single choice of the vertical distribution of the effective static stability. In contrast, wave-CISK theory must choose three different vertical distributions of the heating parameter to obtain different unstable vertical modes.

In contrast to the 40–50-day mode, however, the growth rates of the 25–30- and 10–20-day modes in the present quasi-linear model are too weak to explain the results of the control experiments conducted in Part I, using a fully nonlinear model incorporating the original scheme of MCA. According to these experiments, both the 40–50- and 25–30-day TIOs are maintained primarily through the EWF mechanism, while the 10–20-day Kelvin wave is maintained primarily through the ST mechanism. It is then speculated that the 25–30-day mode can strongly grow through the nonlinear EWF mechanism in a fully nonlinear model, while the 10–20-day mode can strongly amplify through the ST mechanism in a model that fully incorporates diagnostic- and prognostic-adjustment processes.

To examine the above speculations, the control experiments conducted in Part I have been extended to study the full nonlinear effects of conditional heating and evaporation-wind feedback. As will be reported in a subsequent paper, it was found that conditional heating decreases the periods of the TIOs and suppresses high-wavenumber components, consistent with the results of the present quasi-linear EWF theory. Conditional heating also enhances the 25–30-day TIO, consistent with the present speculation. It was also found that stronger basic easterlies in the evaporation scheme result in shorter period TIOs, consistent with the present results.

The present quasi-linear model with prognostic adjustment should be improved by incorporating

many vertical levels with realistic stratification, latitudinal dependence, the earth's rotation, and a boundary layer. The fully nonlinear effects of conditional heating, evaporation-wind feedback, and advection should also be incorporated, with the zonal mean state in the convective layer relaxed toward conditionally neutral and saturated values.

It was proposed in Section 5 that gravity waves, cloud clusters, and superclusters are generated through the "non-resonant" ST mechanism, while Kelvin and MRG waves are resonantly amplified through the "resonant" ST mechanism. The former mechanism should be studied by the use of the original MCA scheme that incorporates both diagnostic- and prognostic-adjustment processes. The latter mechanism can be studied by replacing the diagnostic-adjustment scheme in the perturbation equations with random forcing.

Acknowledgments

The authors are grateful to Drs. S. Manabe and J.D. Mahlman for their advice and encouragement. Appropriate comments on the original manuscript were offered by Drs. I.M. Held, K. Hamilton, and H. Itoh. Discussion with Dr. A. Numaguti was profitable in improving the dynamical interpretation of the united mechanisms. Valuable suggestions from anonymous reviewers were gratefully appreciated. Thank are extended to Ms. Wendy Marshall for her excellent typing.

Appendix A
List of Symbols

t	time
x	zonal coordinate
z	vertical log-pressure coordinate
z_T	height of the convective layer
ϕ	geopotential
p	pressure
ρ	density
u	eastward velocity
v	northward velocity
w	upward velocity in log-pressure coordinates
$T,q,\boldsymbol{H}$	temperature, specific humidity, and temperature-moisture vector
h	moist static energy
$Q_T,Q_q,\boldsymbol{Q}_a$	heating, moistening, and heating-moistening vector, due to convective adjustment
$D_T,D_q,\boldsymbol{D}_a$	same as in the above, except due to diagnostic adjustment
$P_T,P_q,\boldsymbol{P}_a$	same as in the above, except due to prognostic adjustment
$F_T,F_q,\boldsymbol{F}$	same as in the above, except not due to convective adjustment
V_T,V_q	vertical diffusion of static energy and moisture
E	surface evaporation
C_p	specific heat of air at constant pressure
L	latent heat of condensation per unit mass of water vapor
R	gas constant for dry air
H	scale-height constant in the log-pressure coordinate system
γ	temperature-derivative of saturated specific humidity
ε	heating-amplitude reduction factor due to conditional heating
S_T	static stability
S_q	vertical gradient of specific humidity
$\overline{S}_e$	effective static stability
N	buoyancy frequency
A_e	effective evaporation-wind feedback coefficient
$\langle\rangle$	vertical mass-average
$\tilde{(\ )}$	average over time increment Δt
$\hat{(\ )}$	temporarily predicted value without adjustment
$\bar{(\ )}$	basic state
$(\ )'$	deviation from the basic state
$(\ )^*$	saturated value
σ	complex frequency
k	zonal wavenumber

Appendix B
Determination of the Partitioned Scheme

a. The prognostic adjustment

The heating $\tilde{\boldsymbol{P}}_T$ and moistening $\tilde{\boldsymbol{P}}_q$ due to prognostic adjustment presented in Section 2 are determined by the set of Eqs. (2.9a)–(2.9b) in which $\tilde{\boldsymbol{Q}}_a$

and $\boldsymbol{H}(t)$ are replaced by $\tilde{\boldsymbol{P}}_a$ and $\boldsymbol{H}_a(t)$, respectively. The replaced equations in differential form are given by

$$C_p\frac{\partial T_a}{\partial t} = F_T + P_T, \tag{B1a}$$

$$L\frac{\partial q_a}{\partial t} = F_q + P_q, \tag{B1b}$$

$$\frac{\partial}{\partial z}(C_pT_a + Lq_a + \phi_a) = 0, \tag{B1c}$$

$$q_a = q^*(T,p) \text{ at } T = T_a, \tag{B1d}$$

and

$$\langle P_T + P_q\rangle = 0. \tag{B1e}$$

Equation (B1c), when employing the hydrostatic approximation, yields

$$\frac{\partial}{\partial z}(C_pT_a + Lq_a) + \frac{R}{H}T_a = 0. \tag{B2}$$

On the other hand, differentiating (B1d) with respect to time gives

$$L\frac{\partial q_a}{\partial t} = \gamma C_p\frac{\partial T_a}{\partial t}, \tag{B3a}$$

Here, γ is defined by

$$\gamma = \frac{L}{C_p}\frac{\partial q^*}{\partial T} \text{ at } T = \overline{T}(z), \tag{B3b}$$

where $\overline{T}(z)$ is the basic adjusted temperature prescribed as a function of z. Differentiating (B2) with respect to time results in

$$\frac{\partial}{\partial z}\left[C_p(1+\gamma)\frac{\partial T_a}{\partial t}\right] + \frac{R}{H}\left(\frac{\partial T_a}{\partial t}\right) = 0, \tag{B4}$$

where use has been made of (B3a).

Eliminating P_T and P_q from (B1e) by the use of (B1a), (B1b), and (B3a) yields

$$\langle C_p(1+\gamma)\frac{\partial T_a}{\partial t}\rangle = \langle F_T + F_q\rangle. \tag{B5}$$

The tendencies $\frac{\partial T_a}{\partial t}$ and $\frac{\partial q_a}{\partial t}$ can be determined by solving the first-order differential equation (B4) with respect to z, under the constraint given in (B5) as

$$C_p\frac{\partial T_a}{\partial t} = \frac{1}{1+\gamma}\cdot\frac{e(-z)}{\langle e(-z)\rangle}\langle F_T + F_q\rangle, \tag{B6a}$$

and

$$L\frac{\partial q_a}{\partial t} = \frac{\gamma}{1+\gamma}\cdot\frac{e(-z)}{\langle e(-z)\rangle}\langle F_T + F_q\rangle, \tag{B6b}$$

where

$$e(z) = \exp\left[\int_0^z \frac{R}{C_pH(1+\gamma)}dz\right]. \tag{B6c}$$

The desired P_T and P_q are then determined by (B1a) and (B1b) as

$$P_T = C_p\frac{\partial T}{\partial t} - F_T, \tag{B7a}$$

and

$$P_q = L\frac{\partial q_a}{\partial t} - F_q, \tag{B7b}$$

where $\frac{\partial T_a}{\partial t}$ and $\frac{\partial q_a}{\partial t}$ are explicitly given by (B6a) and (B6b), respectively.

b. The diagnostic adjustment

Similarly, the heating D_T and moistening D_q due to diagnostic adjustment are determined by the set of equations (2.9a)–(2.9d), in which $\tilde{\boldsymbol{Q}}_a$, $\boldsymbol{H}_a(t+\Delta t)$, and $\hat{\boldsymbol{H}}(t+\Delta t)$ are replaced by $\tilde{\boldsymbol{D}}_a$, $\boldsymbol{H}_a(t)$, and $\boldsymbol{H}(t)$, respectively. Eliminating $\tilde{D}_T$ and $\tilde{D}_q$, the replaced equations are reduced to

$$\frac{\partial}{\partial z}[C_p(1+\gamma)(T_a - T)] + \frac{R}{H}(T_a - T) = -\frac{\partial h}{\partial z}, \tag{B8a}$$

$$L(q_a - q) = \gamma C_p(T_a - T), \tag{B8b}$$

and

$$\langle(1+\gamma)(T_a - T)\rangle = 0, \tag{B8c}$$

where q is saturated at the onset of diagnostic adjustment, while $T_a - T$ is assumed to be sufficiently small for the approximate moisture-temperature relation (B8b) to be valid.

Solving the first-order differential equation (B8a) under the constraint (B8c) yields

$$(1+\gamma)C_p(T_a - T) = \frac{e(-z)}{\langle e(-z)\rangle}\langle h_e\rangle - h_e, \tag{B9a}$$

where $e(z)$ has been defined by (B6c), and h_e defined as

$$h_e(z) = e(-z)\int_0^z \frac{\partial h}{\partial z}e(z)dz. \tag{B9b}$$

The desired $\tilde{D}_T$ and $\tilde{D}_q$ are then obtained by use of (2.12a) as

$$\tilde{D}_T\Delta t = \frac{1}{1+\gamma}\left[\frac{e(-z)}{\langle e(-z)\rangle}\langle h_e\rangle - h_e\right], \tag{B10a}$$

$$\tilde{D}_q\Delta t = \frac{\gamma}{1+\gamma}\left[\frac{e(-z)}{\langle e(-z)\rangle}\langle h_e\rangle - h_e\right]. \tag{B10b}$$

Appendix C
Finite-Difference Equations

The finite-difference equations for (3.6a) and (3.6b) (see Fig. 5) are written as

$$\lambda[(w_3 + w_4)/2 - 2w_4] + S_4w_4 = 0, \tag{C1a}$$

$$\lambda[(w_2 + w_3)/2 + (w_3 + w_4)/2 - 2w_3] + S_3w_4 = 0, \tag{C1b}$$

$$\lambda[(w_1 + w_2)/2 + (w_2 + w_3)/2 - 2w_2] + S_2w_2 + iA_2w_1 = 0, \tag{C1c}$$

and

$$\lambda[(w_1 + w_2)/2 - 2w_1] + S_1 w_1 + iA_1 w_1 = 0, \quad \text{(C1d)}$$

where

$$\lambda = \left(\frac{\sigma}{h\Delta z}\right)^2. \quad \text{(C1e)}$$

Here, A_1 and A_2 are defined as

$$A_1 = A_2 = \frac{1}{1+\gamma} \cdot \frac{A_e}{k\Delta z} \cdot \frac{R}{H}, \quad \text{(C2a)}$$

where

$$\Delta_z = z_T/4. \quad \text{(C2b)}$$

The eigenvalues λ are determined such that the determinant of the above linear algebraic equations becomes zero, written as

$$B_4\lambda^4 + B_3\lambda^3 + B_2\lambda^2 + B_1\lambda + B_0 = 0, \quad \text{(C3a)}$$

where

$$B_4 = 8, \quad \text{(C3b)}$$

$$B_3 = -(7S_1 + 15S_2 + 15S_3 + 7S_4) - 5iA_2, \quad \text{(C3c)}$$

$$B_2 = 10S_1S_2 + 12S_1S_3 + 6S_1S_4 + 18S_2S_3 + 12S_2S_4 + 10S_3S_4 + iA_2(6S_3 + 4S_4), \quad \text{(C3d)}$$

$$B_1 = -(12S_1S_2S_3 + 8S_1S_2S_4 + 8S_1S_3S_4 + 12S_2S_3S_4) - 4iA_2S_3S_4, \quad \text{(C3e)}$$

and

$$B_0 = 8S_1S_2S_3S_4. \quad \text{(C3f)}$$

Here,

$$S_1 = (1-\varepsilon)\overline{S}_1 + iA_1, \quad \text{(C4a)}$$

$$S_2 = (1-\varepsilon)\overline{S}_2, \quad \text{(C4b)}$$

$$S_3 = \overline{S}_3, \quad \text{(C4c)}$$

and

$$S_4 = \overline{S}_4. \quad \text{(C4d)}$$

References

Arakawa, A., 1993: *Closure assumptions in the cumulus parameterization problem.* Meteorological Monographs, Vol. 24, No. 46, *Amer. Meteor. Soc.*, pp. 1–15.

Arakawa, A. and J.-M. Chen, 1987: Closure assumptions in the cumulus parameterization problem. Short- and Medium-Range Numerical Weather Prediction: Collection of Papers Presented at the WMO/IUGG NWP Symposium, Tokyo, August 1986. Special volume of *J. Meteor. Soc. Japan*, 107–131.

Arakawa, A. and W.H. Schubert, 1974: Interaction of a cumulus cloud ensemble with the large-scale environment. Part I. *J. Atmos. Sci.*, **31**, 674–701.

Arakawa, A. and K.-M. Xu, 1992: The macroscopic behavior of simulated cumulus convection and semi-prognostic tests of the Arakawa-Schubert cumulus parameterization. In *Physical Process in Atmospheric Models.* O.R. Sikka and S.S. Singh, Eds., *Wiley Eastern Limited*, 3–18.

Bates, J.R., A.M. Lasheen and A.F. Hanna, 1978: On the application of the Arakawa-Schubert convective parameterization scheme. *J. Atmos. Sci.*, **35**, 1043–1046.

Bergman, J.W. and M.L. Salby, 1994: Equatorial wave stability derived from fluctuations in observed convection. *J. Atmos. Sci.*, **51**, 3791–3806.

Betts, A.K., 1986: A new convective adjustment scheme. Part I: Observational and theoretical basis. *Quart. J. Roy. Meteor. Soc.*, **112**, 677–691.

Betts, A.K. and M.J. Miller, 1986: A new convective adjustment scheme. Part II: Single column tests using GATE waves, BOMEX, ATEX and arctic air-mass data sets. *Quart. J. Roy. Meteor. Soc.*,**112**, 693–709.

Brown, R.G. and C.S. Bretherton, 1995: Tropical wave instabilities: Convective interaction with dynamics using the Emanuel convective parameterization. *J. Atmos. Sci.*, **52**, 67–82.

Cohn, S.E. and D.P. Dee, 1989: An analysis of the vertical structure equation for arbitrary thermal profiles. *Quart. J. Roy. Meteor. Soc.*, **115**, 143–171.

Crum, F.X. and T.J. Dunkerton, 1992: Analytic and numerical models of wave-CISK with conditional heating. *J. Atmos. Sci.*, **49**, 1693–1708.

Crum, F.X. and T.J. Dunkerton, 1994: CISK and evaporation-wind feedback with conditional heating of an equatorial beta-plane. *J. Meteor. Soc. Japan*, **72**, 11–18.

Dunkerton, T.J. and F.X. Crum, 1991: Scale selection and propagation of wave-CISK with conditional heating. *J. Meteor. Soc. Japan*, **69**, 449–458.

Emanuel, K.A., 1987: An air-sea interaction model of intraseasonal oscillations in the tropics. *J. Atmos. Sci.*, **44**, 2324–2340.

Emanuel, K.A., 1991: A scheme for representing cumulus convection in large-scale models. *J. Atmos. Sci.*, **21**, 2313–2335.

Emanuel, K.A., 1994: *Atmospheric Convection. Oxford University Press*, New York, 580 pp.

Emanuel, K.A., J.D. Neelin, and C.S. Bretherton, 1994: On large-scale circulations in convecting atmospheres. *Quart. J. Roy. Meteor. Soc.*, **120**, 1111–1143.

Emanuel, K.A. and D.J. Raymond, 1993: *The Representation of Cumulus Convection in Numerical Models.* Meteorological Monograph, Vol. 24, No. 46, *Amer. Meteor. Soc.*, 246 pp.

Farrell, B.F., 1989: Optimum excitation of baroclinic waves. *J. Atmos. Sci.*, **46**, 1193–1206.

Farrell, B.F. and P.J. Ioannou, 1996a: Generalized stability theory. Part I: Autonomous operators. *J. Atmos. Sci.*, **53**, 2025–2040.

Farrell, B.F. and P.J. Ioannou, 1996b: Generalized stability theory. Part II: Nonautonomous operators. *J. Atmos. Sci.*, **53**, 2041–2053.

Gadd, A.J., and J.F. Keers, 1970: Surface exchanges of

sensible and latent heat in a 10-level model atmosphere. *Quart. J. Roy. Meteor. Soc.*, **96**, 297–308.

Gill, A.E., 1982: *Atmosphere-Ocean Dynamics.* Academic Press, 662 pp.

Goswami, P. and R.K. Rao, 1994: A dynamical mechanism for selective excitation of the Kelvin mode at timescale of 30–50 days. *J. Atmos. Sci.*, **51**, 2769–2779.

Goswami, P. and V. Mathew, 1994: A mechanism of scale selection in tropical circulation at observed intraseasonal frequencies. *J. Atmos. Sci.*, **51**, 3153–3160.

Hack, J.J., 1994: Parameterization of moist convection in the National Center for Atmospheric Research community climate model (CCM2). *J. Geophys. Res.*, **99**, 5551–5568.

Hayashi, Y., 1970: A theory of large-scale equatorial waves generated by condensational heat and accelerating the zonal wind. *J. Meteor. Soc. Japan*, **48**, 140–160.

Hayashi, Y., 1971a: Instability of large-scale equatorial waves under the radiation condition. *J. Meteor. Soc. Japan*, **49**, 316–319.

Hayashi, Y., 1971b: Large-scale equatorial waves destabilized by convective heating in the presence of surface friction. *J. Meteor. Soc. Japan*, **49**, 458–466.

Hayashi, Y., 1976: Non-singular resonance of equatorial waves under the radiation condition. *J. Atmos. Sci.*, **33**, 183–201.

Hayashi, Y. and D.G. Golder, 1994: Kelvin and mixed Rossby-gravity waves appearing in the GFDL "SKYHI" general circulation model and the FGGE dataset: Implications for their generation mechanism and role in the QBO. *J. Meteor. Soc. Japan*, **72**, 901–935.

Hayashi, Y. and D.G. Golder, 1997: United mechanisms for the generation of low- and high-frequency tropical waves. Part I: Control experiments with moist convective adjustment. *J. Atmos. Sic.*, **54**, 1262–1276.

Hayashi, Y., D.G. Golder and J.D. Mahlman, 1984: Stratospheric and mesospheric Kelvin waves simulated by the GFDL "SKYHI" general circulation model. *J. Atmos. Sci.*, **41**, 1971–1984.

Hendon, H.H. and B. Liebmann, 1991: The structure and annual variation of antisymmetric fluctuations of tropical convection and their association with Rossby-gravity waves. *J. Atmos. Sci.*,**48**, 2127–2140.

Hirota, I., 1978: Equatorial waves in the upper stratosphere and mesosphere in relation to the semiannual oscillation of the zonal wind. *J. Atmos. Sci.*, **35**, 714–722.

Horinouchi, T. and S. Yoden, 1996: Excitation of transient waves by localized episodic heating in the tropics and their propagation into the middle atmosphere. *J. Meteor. Soc. Japan*, **74**, 189–210.

Itoh, H., 1977: The response of equatorial waves to thermal forcing. *J. Meteor. Soc. Japan*, **55**, 222–239.

Itoh, H., 1989: The mechanism for the scale selection of tropical intraseasonal oscillations. Part I: Selection of wavenumber 1 and the three-scale structure. *J. Atmos. Sci.*, **46**, 1779–1798.

Kuo, H.-L., 1965: On formation and intensification of the tropical cyclones through latent heat release by cumulus convection. *J. Atmos. Sci.*, **22**, 40–63.

Kuo, H.-L., 1974: Further studies of the parameterization of the influence of cumulus convection on large-scale flow. *J. Atmos. Sci.*, **31**, 1232–1240.

Kurihara, Y., 1973: A scheme of moist convective adjustment. *Mon. Wea. Rev.*, **95**, 441–451.

Lau, K.-M. and L. Peng, 1987: Origin of low frequency (intraseasonal) oscillations in the tropical atmosphere. Part I: Basic theory. *J. Atmos. Sci.*, **44**, 950–972.

Lau, K.-M. and S. Shen, 1988: On the dynamics of intraseasonal oscillations and ENSO. *J. Atmos. Sci.*, **45**, 1781–1797.

Manabe, S., J. Smagorinsky and R.F. Stricler, 1965: Simulated climatology of a general circulation model with a hydrologic cycle. *Mon. Wea. Rev.*, **93**, 769–798.

Manzini, E. and K. Hamilton, 1993: Middle atmospheric traveling waves forced by latent heat and convective heating. *J. Atmos. Sci.*, **50**, 2180–2200.

Miyahara, S., 1987: A simple model of the tropical intraseasonal oscillation. *Quart. J. Meteor. Soc. Japan*, **65**, 341–351.

Neelin, J.D. and I.M. Held, 1987: Modeling tropical convergence based on the moist static energy budget. *Mon. Wea. Rev.*, **113**, 3–12.

Neelin, J.D. and J.-Y. Yu, 1994: Modes of tropical variability under convective adjustment and the Madden-Julian oscillation. Part I: Analytical theory. *J. Atmos. Sci.*, **51**, 1876–1894.

Neelin, J.D., I.M. Held and K.H. Cook, 1987: Evaporation-wind feedback and low-frequency variability in the tropical atmosphere. *J. Atmos. Sci.*, **44**, 2341–2348.

Numaguti, A. and Y. Hayashi, 1997: Gravity-wave dynamics of the hierarchical structure of super cloud clusters (submitted for publication).

Ohuchi, K. and M. Yamasaki, 1997: Kelvin wave-CISK controlled by surface friction; a possible mechamism of super cloud cluster. Part I: Linear theory. *J. Meteor. Soc. Japan*, **75**, 497–511.

Randall, D.A. and D.-M. Pan, 1993: *Implementation of the Arakawa-Schubert cumulus parameterization with a prognostic closure.* Meteorological Monograph, Vol. 24, No. 46, *Amer. Meteor. Soc.*, pp. 137–144.

Salby, M.L. and H.H. Hendon, 1994: Planetary-scale circulations in the presence of climatological and wave-induced heating. *J. Atmos. Sci.*, **51**, 2344–2367.

Salby, M.L., D.L. Hartmann, P.L. Baily and J.C. Gille, 1984: Evidence for equatorial Kelvin modes in Nimbus 7 LIMS. *J. Atmos. Sci.*, **41**, 220–235.

Trefethen, L.N., A.E. Trefethen, S.C. Reddy, and T.A. Driscoll, 1993: Hydrodynamical stability without eigenvalues. *Science*, **261**, 578–584.

Wang, B., 1988: Dynamics of the tropical low-frequency waves: An analysis of the moist Kelvin waves. *J. Atmos. Sci.*, **45**, 2051–2065.

Xie, S.-P., 1994: On the preferred zonal scale of wave-CISK with conditional heating. *J. Meteor. Soc. Japan*, **72**, 19–30.

Xie, S.-P. and A. Kubokawa, 1990: On the wave-CISK in the presence of the boundary layer. *J. Meteor. Soc. Japan*, **68**, 651–657.

Xie, S.-P., A. Kubokawa and K. Hanawa, 1993a: Evaporation-wind feedback and the organizing of tropical convection on the planetary scale. Part I. Quasi-linear instability. *J. Atmos. Sci.*, **50**, 3873–3883.

Xie, S.-P., A. Kubokawa and K. Hanawa, 1993b: Evaporation-wind feedback and the organizing of tropical convection on the planetary scale. Part II. Nonlinear evolution. *J. Atmos. Sci.*, **50**, 3884–3893.

Yoshizaki, M., 1991: Selective amplification of the eastward-propagating mode in a positive-only wave-CISK model on an equatorial beta-plane. *J. Meteor. Soc. Japan*, **69**, 353–373.

Yu, J.-Y. and J.D. Neelin, 1994: Modes of tropical variability under convective adjustment and the Madden-Julian oscillation. Part II: Numerical results. *J. Atmos. Sci.*, **51**, 1895–1914.

低・高周波熱帯波動の生成のための連合機構 第II部：理論的解釈

林　良一・D.G. Golder

（プリンストン大学地球流体力学研究所）

低・高周波熱帯波動は、蒸発一風フィードバック (Evaporation — wind feedback, EWF)、飽和トリッガー (saturation triggering, ST) および中緯度からのトリッガー (lateral triggering) からなる連合機構 (united mechanisms) により生成されると見なされる。EWF メカニズムは、ある種の波が蒸発一風フィードバックによって不安定になる。ST メカニズムは、別の種類の波が飽和とともに湿潤対流の断続的開始によりトリッガーされ、すでに存在していた条件付き不安定成層を中立化させる。これらのメカニズムは、理論的には湿潤対流調節によって診断的 (diagnostic) および予測的 (prognostic) 調節という二つの一貫した過程として説明される。この二つの過程は、対流平衡をそれぞれ再生および維持し、STおよびEWF メカニズムに決定的なものである。

一体化された理論へのステップとしてEWF不安定を理論的ケルビン波モデルを用いることによって調べる。このモデルは線形摂動方程式において予測調節過程のみを組み込み、これによってSTメカニズムを除外する。この解は波動不安定がEWFメカニズムの結果であることを示し、波動 — CISKメカニズムではないことを示す。調節パラメーターをもっともらしく選ぶと一つの強い不安定モードが観測上の 40–50 日振動に対応し、二つの弱い不安定モードが25–30日および 10–20日振動に対応する。

これらの結果を、元々の湿潤対流調節スキームを組み込んだ非線形モデルを用いて、第I部で扱っている数値実験からの結果と比較した。推測されることは、40–50日および25–30日モードはそれぞれ線形および非線形EWFメカニズムを通して強く発達しうるのに対し、10–20日モードはSTメカニズムを通して強く増幅しうることである。